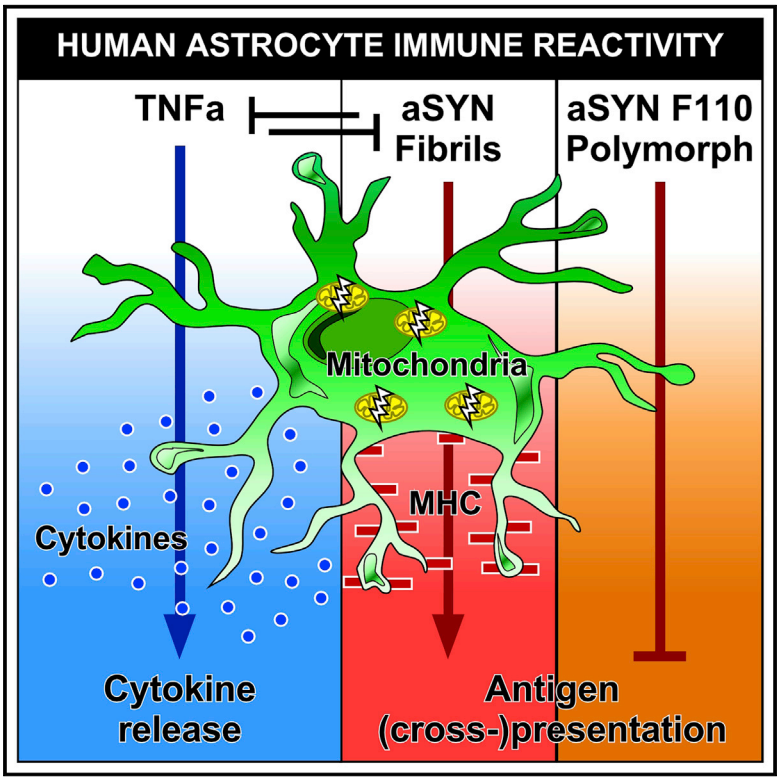
Cell Reports



# TNF-α and α-synuclein fibrils differently regulate human astrocyte immune reactivity and impair mitochondrial respiration

## Graphical abstract




## Highlights

- Astrocytes exposed to TNF-α, but not αSYN fibrils, release pro-inflammatory cytokines
- Astrocytes exposed to αSYN fibrils become antigen (cross)-presenting cells
- Antigen (cross) presentation is hampered by large F110 fibrils
- Astrocytes exposed to TNF-α or αSYN fibrils have impaired mitochondrial respiration

## Authors

Kaspar Russ, Gabriel Teku, Luc Bousset, ..., Mauno Vihinen, Ronald Melki, Laurent Roybon

## Correspondence

laurent.roybon@med.lu.se

## In brief

Russ et al. show that human astrocytes adopt different reactive immune phenotypes when exposed to either TNF-α or alpha-synuclein fibrils, which are exogenous stressors that compete to drive the astrocyte immune reactive response. They also show that *PARK2*-variant-containing astrocytes exhibit an exacerbated response to the stressors, accompanied by bioenergetic defects.

Russ et al., 2021, Cell Reports *34*, 108895
March 23, 2021 © 2021 The Authors.
https://doi.org/10.1016/j.celrep.2021.108895

Cell Reports

CellPress
OPEN ACCESS

Report

# TNF-α and α-synuclein fibrils differently regulate human astrocyte immune reactivity and impair mitochondrial respiration

Kaspar Russ,[1,2,9] Gabriel Teku,[3,11] Luc Bousset,[4,11] Virginie Redeker,[4,12] Sara Piel,[5,10,12] Ekaterina Savchenko,[1,2] Yuriy Pomeshchik,[1,2] Jimmy Savistchenko,[4] Tina C. Stummann,[8] Carla Azevedo,[1,2] Anna Collin,[6] Stefano Goldwurm,[7] Karina Fog,[8] Eskil Elmer,[5] Mauno Vihinen,[3] Ronald Melki,[4,13] and Laurent Roybon[1,2,13,14,*]

[1]Cell Stem Cell Laboratory for CNS Disease Modeling, Department of Experimental Medical Science, BMC D10, Lund University, 22184 Lund, Sweden
[2]MultiPark and the Lund Stem Cell Center, Lund University, 22184 Lund, Sweden
[3]Protein Structure and Bioinformatics, Department of Experimental Medical Science, BMC B13, Lund University, 22184 Lund, Sweden
[4]Institut Francois Jacob (MIRCen), CEA and Laboratory of Neurodegenerative Diseases, CNRS, 18 Route du Panorama, 92265 Fontenay-Aux-Roses, France
[5]Mitochondrial Medicine, Department of Clinical Sciences Lund, Lund University, 22184 Lund, Sweden
[6]Office for Medical Services/division of Laboratory Medicine, Department of Clinical Genetics and Pathology, Lund, Sweden
[7]Centro Parkinson/Parkinson Institute, ASST "Gaetano Pini/CTO," via Bignami 1, 20126 Milan, Italy
[8]H. Lundbeck A/S, Valby, Denmark
[9]Present address: H. Lundbeck A/S, Valby, Denmark
[10]Present address: Center for Mitochondrial and Epigenomic Medicine, Department of Anesthesiology and Critical Care Medicine, Children's Hospital of Philadelphia, Philadelphia, PA 19104-4302, USA
[11]These authors contributed equally
[12]These authors contributed equally
[13]Senior author
[14]Lead contact
*Correspondence: laurent.roybon@med.lu.se
https://doi.org/10.1016/j.celrep.2021.108895

## SUMMARY

Here, we examine the cellular changes triggered by tumor necrosis factor alpha (TNF-α) and different alpha-synuclein (αSYN) species in astrocytes derived from induced pluripotent stem cells. Human astrocytes treated with TNF-α display a strong reactive pro-inflammatory phenotype with upregulation of pro-inflammatory gene networks, activation of the nuclear factor κB (NF-κB) pathway, and release of pro-inflammatory cytokines, whereas those treated with high-molecular-weight αSYN fibrils acquire a reactive antigen (cross)-presenting phenotype with upregulation of major histocompatibility complex (MHC) genes and increased human leukocyte antigen (HLA) molecules at the cell surface. Surprisingly, the cell surface location of MHC proteins is abrogated by larger F110 fibrillar polymorphs, despite the upregulation of MHC genes. Interestingly, TNF-α and αSYN fibrils compete to drive the astrocyte immune reactive response. The astrocyte immune responses are accompanied by an impaired mitochondrial respiration, which is exacerbated in Parkinson's disease (PD) astrocytes. Our data provide evidence for astrocytic involvement in PD pathogenesis and reveal their complex immune reactive responses to exogenous stressors.

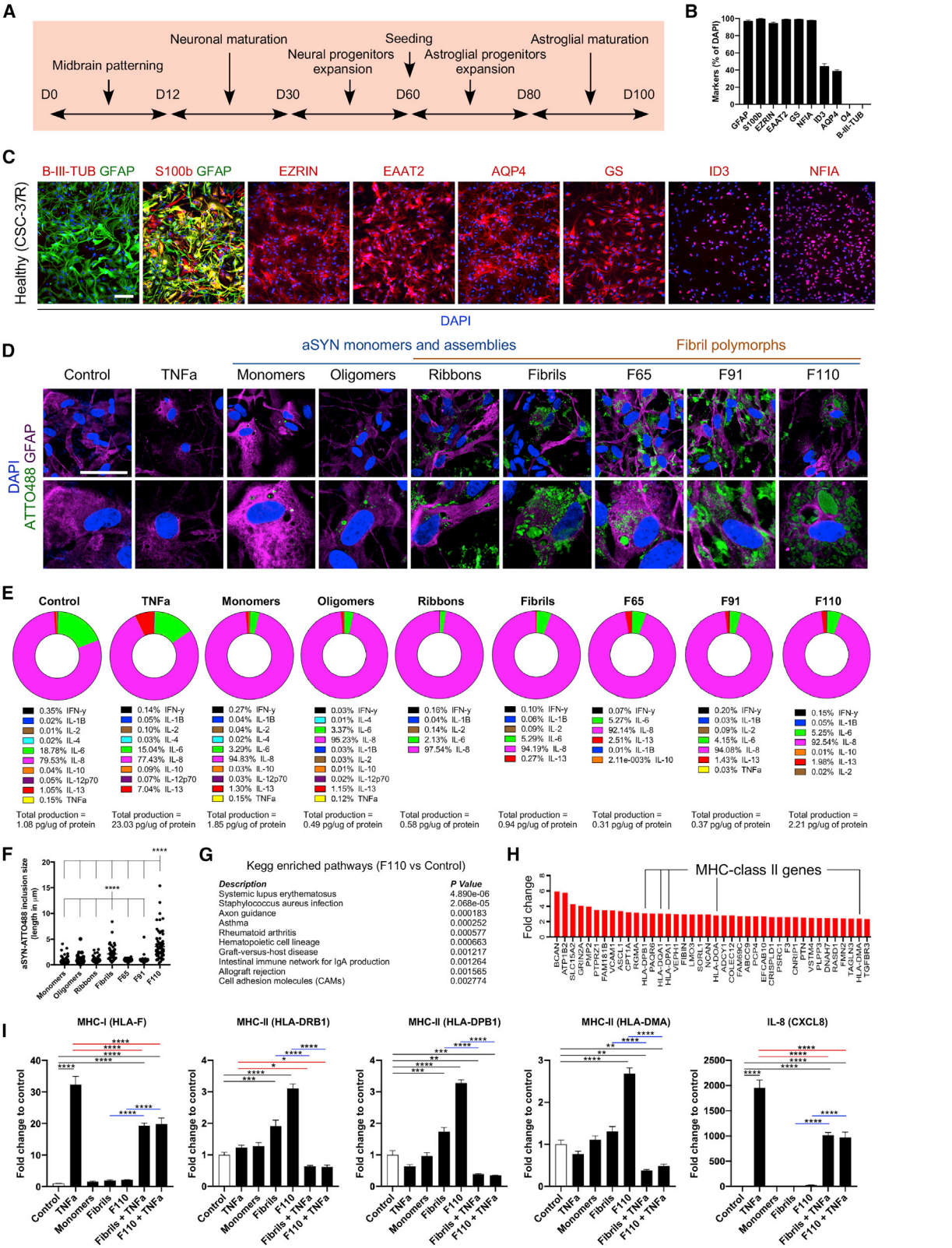
## INTRODUCTION

Parkinson's disease (PD) is a multifactorial neurodegenerative disorder characterized, in part, by the death of pigmented midbrain dopaminergic neurons located in the *substantia nigra pars compacta* (*SNpc*), resulting in motor and non-motor dysfunctions that are prominent at advanced disease stages (Poewe et al., 2017). The major neuropathological characteristics of PD are the presence of alpha-synuclein (αSYN)-containing Lewy bodies in injured neurons and neuroinflammation in the *SNpc* (Spillantini et al., 1997, 1998).

αSYN is a 14-kDa protein encoded by the *SNCA* gene, which under disease conditions can oligomerize into a wide range of high-molecular-weight (MW) oligomers, of which some are fibrillar in nature. They have well-defined structures and properties and exhibit distinct seeding and propagation propensities *in vivo* (Bousset et al., 2013; Guerrero-Ferreira et al., 2019; Li et al., 2018; Makky et al., 2016; Peelaerts et al., 2015; Sun et al., 2020).

αSYN has been observed in immune reactive astrocytes in PD patients' brains (Braak et al., 2007). However, it is not known how different αSYN species that may be present in the PD brain can


This is an open access article under the CC BY-NC-ND license (http://creativecommons.org/licenses/by-nc-nd/4.0/).




*(legend on next page)*

influence glial immune reactivity and function. Answering this question would provide invaluable insight into how αSYN, inflammation, and astrocytes interact in PD pathogenesis. Moreover, because astrocytes express PD-linked genes at levels sometimes similar to neurons (Booth et al., 2017; Zhang et al., 2016), they are expected to exhibit more profound cellular changes than healthy astrocytes, when exposed to aggregated αSYN polymorphs. Such changes might ultimately impact the survival of the neurons they support, particularly dopaminergic neurons.

Uptake of αSYN by rodent astrocytes from neuronally differentiated SH-SY5Y cells overexpressing *SNCA* induced astrocytic expression of genes related to an immune reactive response (Lee et al., 2010). However, it remains to be determined which component of the immune reactive state of the astrocytes was triggered by αSYN, among the factors secreted in response to *SNCA* overexpression. This information would be valuable for the development of therapeutic strategies.

In this study, we investigated whether and how different αSYN species induce human astrocyte immune reactivity.

## RESULTS

### Human iPSC-derived astrocytes exposed to high-MW αSYN species do not release pro-inflammatory cytokines but adopt an antigen (cross)-presenting phenotype

In order to investigate the effect of αSYN species on human astrocytic immune reactivity, we generated induced pluripotent stem cells (iPSCs) from fibroblasts of two non-demented healthy donors (Figure S1). We differentiated iPSCs into astrocytes by using a protocol that spans 100 days (Figure 1A), which was modified from our previous work (Holmqvist et al., 2015). The cells had an astrocytic morphology and the majority stained positive for canonical astrocyte markers GFAP, S100b, EZRIN, EAAT2, AQP4, GS, ID3, and NFIA (Figures 1B and 1C).

First, we confirmed that the astrocytes generated could become immune reactive pro-inflammatory, following treatment with tumor necrosis factor alpha (TNF-α) (Roybon et al., 2013). Human iPSC-derived astrocytes were treated for 6 days with TNF-α (100 ng/ml), and microarray analysis showed up to 100-fold upregulated expression of pro-inflammatory genes compared to control PBS-treated cultures (Table S1; Figure S2). KEGG pathway enrichment analysis revealed activation of TNF-α, nuclear factor kappa-light-chain-enhancer of activated B cells (nuclear factor κB [NF-κB]), and chemokine signaling pathways—all associated with inflammation (Hsiao et al., 2013). Nuclear translocation of NF-κB and release of pro-inflammatory cytokines (interferon γ [IFN-γ], interleukin-1β [IL-1β], IL-2, IL-4, IL-6, IL-8, IL-10, IL-12p70, and IL-13) in the growth media (Meeuwsen et al., 2003) were confirmed by immunocytochemistry and quantified using a sensitive multiplex immunoassay (Figure S2), respectively.

We next examined whether the astrocytes would become immune reactive pro-inflammatory when exposed to αSYN monomers, oligomers, or different high-MW αSYN fibrillar polymorphs (ribbons; fibrils; and fibril 65 [F65], fibril 91 [F91], and fibril 110 [F110] polymorphs; Figure S3). We used immunocytochemistry to confirm internalization and aggregation of ATTO488-labeled αSYN species (Figure 1D). To our surprise, human astrocytes treated with the different αSYN species did not exhibit nuclear translocation of NF-κB (Figure S4). We therefore assessed the presence of pro-inflammatory cytokines as well as TNF-α in the growth media. We did not discover significant increases in cytokine secretion despite the presence of αSYN-positive aggregates in the astrocytes. The total quantity of cytokines secreted was similar between the different αSYN species treatments and similar to PBS-treated control when compared to TNF-α treated cultures (Figure 1E). To rule out the possibility that the astrocytes had responded earlier or that they lacked the ability to respond, we also examined NF-κB nuclear translocation in human embryonic-stem-cell-derived astrocytes, in a time course study at 1 h, 24 h, and 6 days post-exposure, but found no increase in cytokine secretion (Figure S5).

To further investigate cellular changes triggered by αSYN species in astrocytes, we used microarray analysis and focused on cultures treated with αSYN fibrils and high-MW F110 because these two species resulted in the formation of large cytoplasmic aggregates (Figure 1F). F110 results from a truncated form of αSYN, which is devoid of the 30 C-terminal acidic amino acids

**Figure 1. Healthy iPSC-derived astrocytes secrete minimal pro-inflammatory cytokines but upregulate MHC class II genes in response to αSYN treatment**

(A) Differentiation protocol for generating 100-day-old human astrocytes from iPSCs.

(B) Quantification of astrocytic markers in 100-day-old cultures generated for control iPSC line CSC-37R. Data are mean ± SEM; n = 5.

(C) Representative immunostaining for canonical astrocytic markers at day 100. Scale bar, 100 μm.

(D) Representative confocal images for αSYN-ATTO-488- and GFAP-stained cultures treated with PBS (control), TNF-α, or various αSYN species. Scale bar, 100 μm.

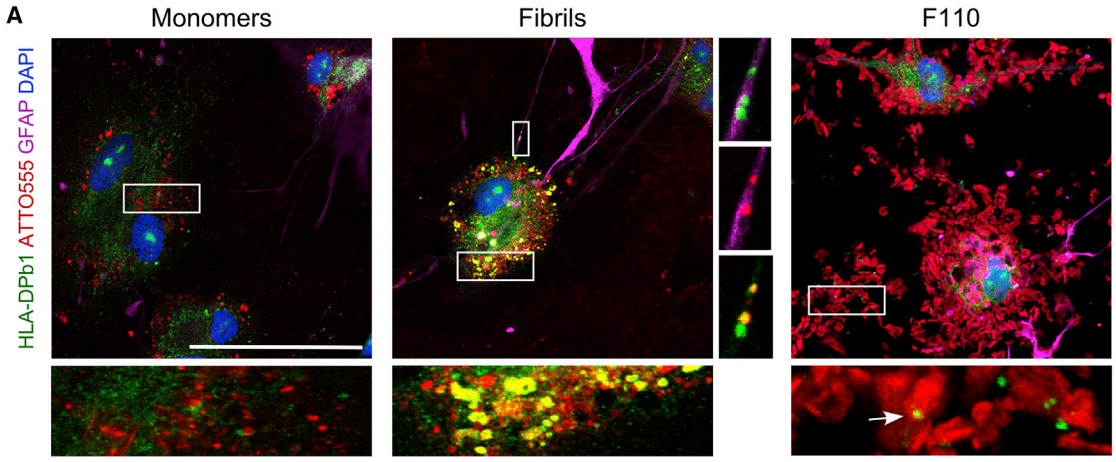
(E) Average total cytokine production (pg/μg protein) following treatment of healthy astrocytes, with individual cytokines displayed as percentage of total production. Data are an average of n = 17 for control (control), n = 8 for monomer-treated group, n = 7 for oligomer-treated group, n = 5 for ribbon-treated group, n = 6 for fibril-treated group, n = 6 for F65-treated group, n = 7 for F91-treated group, and n = 12 for the F110-treated group.

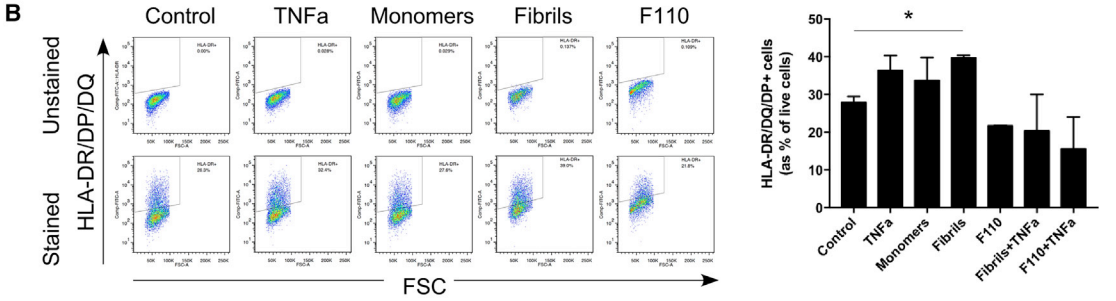
(F) Quantification of the size of the αSYN-ATTO-488-positive inclusions/aggregates present in healthy astrocytes after 6 days of treatment. Each dot represents the length of the aggregate measured. n = 75 aggregates per condition; one-way ANOVA with a Dunnett's multiple comparison test; ****p ≤ 0.0001.

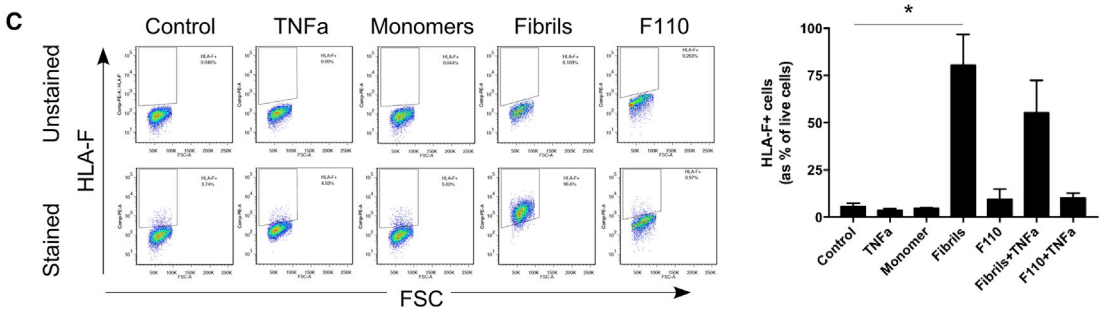
(G) KEGG pathway enrichment analysis shows 10 significantly affected pathways following F110 treatment in healthy astrocytes compared to control. Nine out of 10 pathways contained MHC-class-II-related genes.

(H) Diagram for genes significantly upregulated, in order of fold-change, following F110 treatment of healthy astrocytes compared to control.

(I) qRT-PCR analysis of astrocytes treated with TNF-α, αSYN monomers, αSYN fibrils, αSYN F110, αSYN fibrils and TNF-α, or αSYN F110 and TNF-α for 6 days. Data are mean ± SEM; n = 8 independent experiments per condition. A one-way ANOVA with a Tukey multiple comparison test was used to test the significance for gene fold change in (1) no treatment versus treatment groups (denoted with black line), (2) TNF-α single treatment versus co-treatments (denoted with red line), and (3) αSYN polymorphs single treatment versus co-treatment (denoted with blue line); *p ≤ 0.05, **p ≤ 0.01, ***p ≤ 0.001, ****p ≤ 0.0001.



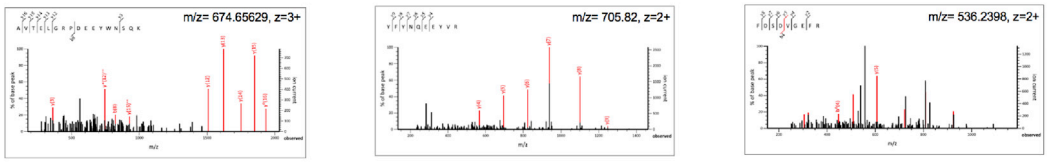




D

| Protein family | Accession | Mascot protein score | Mass | Number of MSMS identifications | Number of identified peptides | Number of unique peptides | Protein description | Species | Gene name |
|---|---|---|---|---|---|---|---|---|---|
| 258 | P01889 | 113 | 40777 | 3 | 2 | 2 | HLA class I histocompatibility antigen, B-7 alpha chain | Homo sapiens | HLA-B |
| 226 | P04233 | 129 | 33950 | 2 | 1 | 1 | HLA class II histocompatibility antigen, gamma chain | Homo sapiens | CD74 |
| 458 | P20039 | 66 | 30483 | 4 | 3 | 3 | HLA class II histocompatibility antigen, DRB1-11 beta chain | Homo sapiens | HLA-DRB1 |

E




F

**13% Sequence protein coverage**

```
  1 MVCLRLPGGS CMAVLTVTLM VLSSPLALAG DTRPRFLEYS TSECHFFNGT
 51 ERVRFLDRYF YNQEEYVRFD SDVGEFRAVT ELGRPDEEYW NSQKDFLEDR
101 RAAVDTYCRH NYGVGESFTV QRRVEPKVTV YPSKTQPLQH HNLLVCSVSG
151 FYPGSIEVRW FRNGQEEKTG VVSTGLIHNG DWTFQTLVML ETVPRSGEVY
201 TCQVEHPSVT SPLTVEWRAR SESAQSKMLS GVGGFVLGLL FLGAGLFIYF
251 RNQKGHSGLQ PRGFLS
```

G

**List of identified peptides**

| Sequence | Peptide | Observed m/z | Mr(expt) | Mr(calc) | ppm | Ion Score |
|---|---|---|---|---|---|---|
| 59-68 | R.YFYNQEEYVR.F | 705.8200 | 1409.6255 | 1409.6252 | 0.22 | 36 |
| 69-77 | R.FDSDVGEFR.A | 536.2398 | 1070.4651 | 1070.4669 | -1.72 | 31 |
| 69-77 | R.FDSDVGEFR.A | 536.2422 | 1070.4698 | 1070.4669 | 2.69 | 20 |
| 78-94 | R.AVTELGRPDEEYWNSQK.D | 674.6563 | 2020.9470 | 2020.9490 | -0.97 | 21 |

*(legend on next page)*

(αSYN 1–110) that can bundle very rapidly prior to and after internalization to cells (Figures 1D and S3). Hardly any genes were upregulated more than 4-fold (Tables S1 and S2). Even after applying a lower 1.5-fold threshold, we found no upregulated genes encoding pro-inflammatory cytokines or chemokines (data not shown; Tables S1 and S2). Interestingly, KEGG enrichment analysis of F110-treated astrocytes did identify pathways associated with major histocompatibility complex (MHC) proteins (Figure 1G). They included human leukocyte antigen (HLA) genes encoding MHC class II proteins, which were significantly upregulated following astrocytic exposure to fibrils and in particular F110 (Figure 1H; Tables S1 and S2).

We used qRT-PCR to confirm the microarray findings and found highly significant altered expression of *HLA-F*, *HLA-DRβ1*, *HLA-DPβ1*, and *HLA-DMA* following the different treatments (Figure 1I). qRT-PCR also confirmed the lack of *CXCL8* gene upregulation following treatment of the astrocytes with αSYN species. Interestingly, co-treatment of the astrocytes with TNF-α and αSYN fibrils or TNF-α and F110 altered the astrocytic expression of *HLA-F*, *HLA-DRβ1*, *HLA-DPβ1*, *CXCL8,* and *HLA-DMA* genes, suggesting that astrocytes had difficulties exhibiting both an immune reactive pro-inflammatory phenotype and an immune reactive antigen-presenting phenotype.

### αSYN fibril peptides interact with MHC proteins in human astrocytes, and αSYN fibrils, but not F110, induce relocation of MHC molecules to the astrocytes surface

The discovery of upregulated HLA genes led us to hypothesize that αSYN fibrils and F110 have antigenic properties in astrocytes. Indeed, we observed that the HLA-DPβ1 staining strongly overlapped with αSYN fibrils (Figure 2A, middle panel), but not with αSYN monomers. This finding suggests that from their entry, and during their accumulation in the astrocytes, most αSYN fibrils were degraded to peptides for antigen presentation. Interestingly, only a few HLA-DPβ1/αSYN F110-positive puncta were observed. However, HLA-DPβ1 was prominently found surrounding the large F110 bundles (Figure 2A, right panel). We speculate that this may be due to the size of F110 bundles and their resistance to proteolytic degradation in astrocytes.

Next, we examined cell surface membrane relocation of MHC class molecules for human astrocytes treated with PBS (control), TNF-α, αSYN monomers, αSYN fibrils, or F110. Interestingly, fluorescence-activated cell sorting (FACS) analysis showed a significant increase in the percentage of MHC-class-II-positive astrocytes in cultures exposed to αSYN fibrils but not in cultures exposed to F110 (Figure 2B). No significant change was identified at the earlier time point (1 day post-treatment; data not shown) despite significantly increased *HLA-DPβ1* gene expression seen 1 day post-treatment (Figure S6). These data indicate that astrocytes had difficulties in degrading the fibrils for presentation by MHC class II molecules and/or that they may have engaged into cross presentation by MHC class I molecules. As limited proteolysis of fibrils has been previously described (Loria et al., 2017; Pieri et al., 2016a), we examined cross presentation. αSYN fibril treatment caused a massive increase in HLA-F-positive astrocytes, despite unchanged mRNA levels (Figures 1I and 2C). These data indicate a relocation of existing HLA-F molecules to the cell surface in astrocytes, either for presentation of αSYN fibril peptides or for open conformer presentation (Dulberger et al., 2017). Interestingly, the increase in *HLA-F* transcripts, mediated by TNF-α treatment, did not translate into increased HLA-F molecules at the astrocyte surface membrane. Additionally, co-treatment of astrocytes with both TNF-α and fibrils antagonized the effect of the fibrils alone on relocation of MHC molecules to the astrocyte cell surface (Figures 2B, 2C, and S6).

To establish whether αSYN fibrils and MHC molecules interact, we treated astrocytes with biotin-labeled αSYN fibrils, prepared membrane fractions, pulled down the fibrils, and identified the associated proteins by using a proteomics approach. Western blot analysis showed the presence of HLA-DPβ1 immuno-reactive bands of different MWs in the membrane fraction in astrocytes treated with the biotinylated αSYN fibrils only. To further demonstrate the MHC protein interaction with αSYN fibrils and to determine which MHC haplotypes interact with αSYN fibrils, we subjected the pulled down astrocyte membrane proteins to trypsin digestion and identified the resulting peptides by nano-LC MS/MS (liquid chromatography-tandem mass spectrometry; Figure S6). Control samples were prepared from astrocytes not exposed to αSYN fibrils as previously described (Shrivastava et al., 2019). We identified 1,020 protein families with at least 1 peptide (mascot ion score of >15) in the membrane

**Figure 2. αSYN-fibril-treated healthy astrocytes acquire an antigen-presenting phenotype and fibril peptides physical interaction with MHC class molecules**

(A) Representative confocal images for astrocyte cultures stained for αSYN-ATTO555, HLA-DPβ1, GFAP, and DAPI, following their exposure to monomers, fibrils, or F110. Extensive colocalization follows fibril treatment only. Scale bar, 100 μm.

(B) Flow cytometry analysis and quantification of HLA-DR/DP/DQ-positive healthy astrocytes treated with either PBS (control), 100 ng/ml TNF-α, or 10 μM αSYN (monomers, fibrils, or F110) for 6 days. Because the treatments changed the morphology of the cells, the percentages of positive cells were calculated using gating for non-stained cells. Data are mean ± SEM; n = 2 independent experiments per condition; t test; *p ≤ 0.05.

(C) Flow cytometry analysis and quantification of HLA-F-positive healthy astrocytes treated with either PBS (control), 100 ng/ml TNF-α, or 10 μM αSYN (monomers, fibrils, or F110) for 6 days. Because the treatments changed the morphology of the cells, the percentages of positive cells were calculated using gating for non-stained cells. Data are mean ± SEM; n = 2 independent experiments per condition; t test; *p ≤ 0.05.

(D) A total of 1,020 and 126 protein families were identified with at least 1 peptide (Mascot ions core ≥ 15) from pull-downs performed on membrane fractions from cells exposed or not to biotinylated αSYN fibrils, respectively. Three MHC protein members were identified in astrocytes exposed to biotinylated αSYN fibrils; two were identified in the MHC class II family. No MHC proteins were detected in untreated astrocytes.

(E) The MS/MS fragmentation spectra of three HLA-DRβ1 (P20039) tryptic peptides identified after pull-down of biotinylated αSYN fibrils. Spectra show primary structure, mascot ion score, *m/z*, and mass accuracy of the fragmented precursor peptide. The primary structure was determined from the y (red) fragment ions.

(F) Primary structure coverage of HLA class II histocompatibility antigen DRβ1-11 beta chain (HLA-DRβ1). The 13% sequence coverage of HLA-DRβ1 is marked in red.

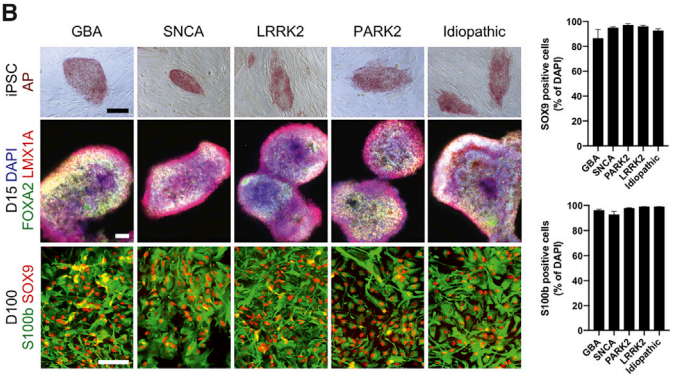
(G) Sequence and properties of the four HLA-DRβ1 tryptic peptides, identified by nano-LC-MS/MS analysis.

**A**

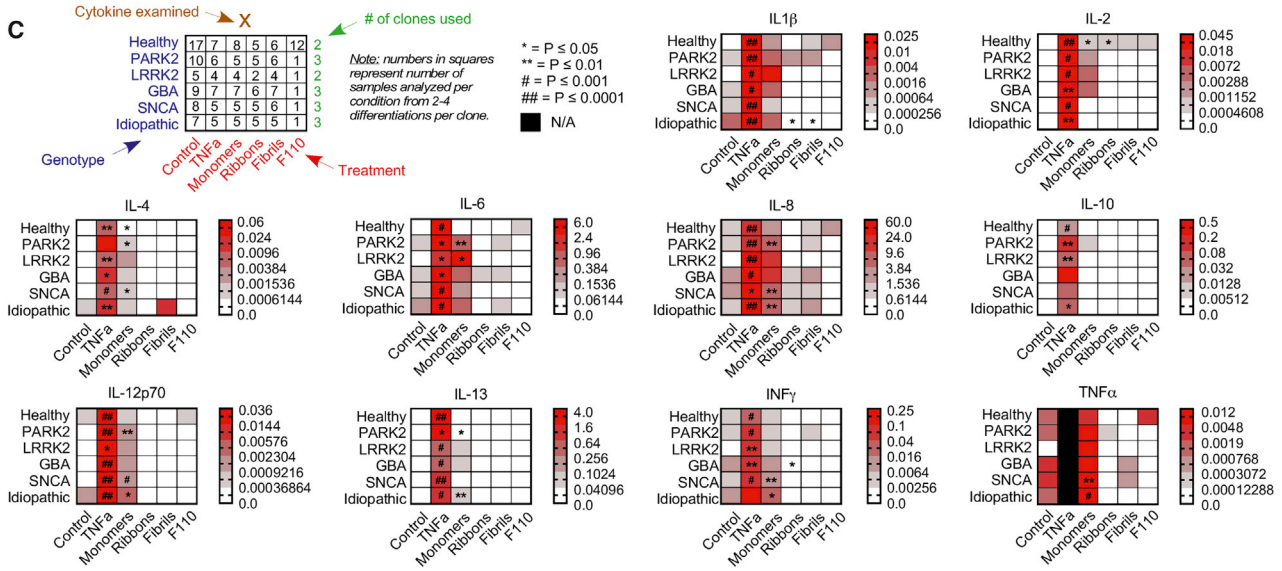
| Clone ID | Diagnosis | Molecular analysis | Gender | Reprogramming | Reference |
|---|---|---|---|---|---|
| CSC-10A | PD (GBA) | *p.L444P/WT* | Female | Sendai virus | 2 |
| CSC-10B | | *p.L444P/WT* | | Sendai virus | 2 |
| CSC-10C | | *p.L444P/WT* | | Sendai virus | 2 |
| CSC-7A | PD (PARK2) | *p.C273W/p.C273W* | Female | Retrovirus | 2 |
| CSC-7B | | *p.C273W/p.C273W* | | Retrovirus | 2 |
| CSC-21B | | *p.A275W/p.A275W* | Female | Sendai virus | 2 |
| CSC-18A | PD (LRRK2) | *p.R1441C/WT* | Male | Sendai virus | 2 |
| CSC-19A | | *p.G2019S/WT* | Male | Sendai virus | 2 |
| CSC-3G | PD (SNCA) | triplication | Female | Retrovirus | 1; 2 |
| CSC-3S | | triplication | | Retrovirus | 1; 2 |
| CSC-28N # | | triplication | | Sendai virus | this study |
| CSC-26B | Idiopathic PD | | Female | Sendai virus | this study |
| CSC-27I | | | Male | Sendai virus | this study |
| CSC-27K | | | | Sendai virus | this study |

# CSC-28N and CSC-3G and -3S are from the same patient, but differently reprogrammed

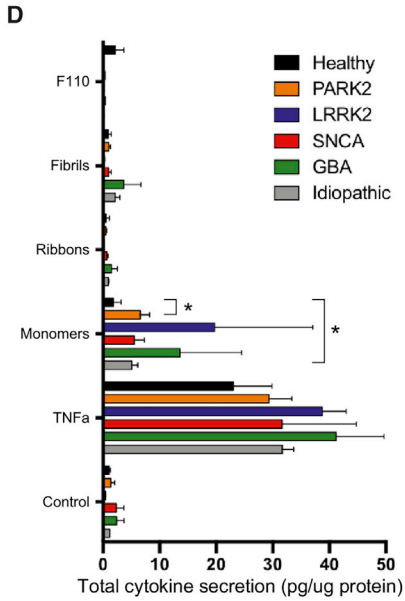
**B**



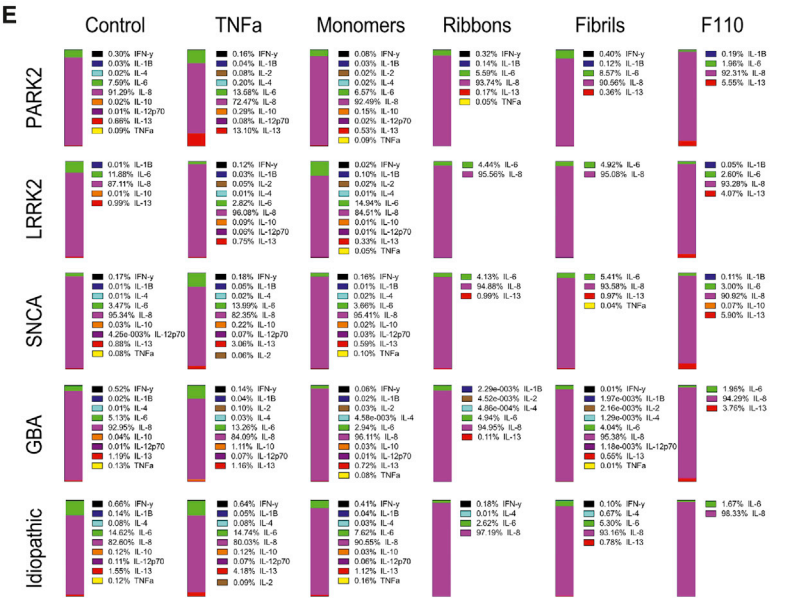

**C**




**D**




**E**




*(legend on next page)*

fraction (Figures 2D and 2E; Table S3). The HLA class II histocompatibility antigen DRβ1-11 beta chain was identified with a high degree of certainty, confirming the interaction between αSYN fibril peptides and MHC molecules (Figures 2F and 2G).

### PD-variant-containing astrocytes display increased production of pro-inflammatory cytokines when exposed to αSYN monomers but not when exposed to αSYN fibrils or F110

A recent study suggested that PD astrocytes may show an exacerbated response to pro-inflammatory stressors (Sonninen et al., 2020). We therefore assessed pro-inflammatory cytokine release from astrocytes differentiated from iPSCs generated from PD patients with genetic variants in *PARK2*, *LRRK2*, *SNCA*, or *GBA*, as well as from patients with idiopathic PD (Figure 3A).

First, we generated iPSCs from the PD variants and idiopathic PD fibroblasts and then differentiated them to astrocytes. By day 15, the neural progenitors acquired a ventral midbrain identity, as confirmed by immunocytochemistry for LMX1A and FOXA2 markers (Figure 3B). By day 100, the cultures were enriched in astrocytes immuno-positive for S100β and SOX9 (Figure 3B). Astrocytes treated with TNF-α released high amounts of pro-inflammatory cytokines, measured using a sensitive multiplex immunoassay (Figure 3C), and relocated NF-κB to the nucleus (Figure S4). PD astrocytes exposed to high MW αSYN species released low total levels of pro-inflammatory cytokines, ranging from 0.44 to 2.39 pg/μg (Figure 3D). However, we found at least a 2-fold increase in secretion of the main pro-inflammatory cytokines IL-6 and IL-8 in PD astrocytes compared to control healthy astrocytes upon exposure to αSYN monomers (Figure 3D). Astrocytes with the *PARK2*-variant background exhibited highly significant changes in pro-inflammatory cytokine production (Figures 3D and 3E).

### High-MW αSYN species impair ATP-generating mitochondrial respiration in healthy and in PARK2-variant PD astrocytes

Recent evidence suggests altered mitochondrial fusion and fragmentation rates following exposure to αSYN fibrils and on-fibrillar assembly pathway oligomers in human neurons and astrocytes derived from pluripotent stem cells (Gribaudo et al., 2019; Rostami et al., 2017). Therefore, we investigated whether the astrocytic exposure to αSYN monomers, fibrils, or F110 would impair mitochondrial function. Untreated cultures, following normalization to citrate synthase activity, had no significant difference in basal, uncoupled, or coupled (ATP generating) respiration in astrocytes when using Seahorse analysis (data not shown). Similar results were obtained when cultures were normalized to the total amount of protein (data not shown). Control (non-PD) astrocytes exposed to αSYN fibrils, but not αSYN monomers or F110, had a significant decrease in basal, uncoupled, and coupled mitochondrial respiration (Figure 4A). Interestingly, *PARK2*-variant PD astrocytes, which showed the most significant change in release of pro-inflammatory cytokines following exposure to αSYN monomers, exhibited a more pronounced decrease in basal, uncoupled, and coupled respiration upon exposure to αSYN fibrils or F110 polymorphs than healthy astrocytes (Figure 4B). Citrate synthase activity was not significantly changed in control and *PARK2*-variant PD astrocytes following addition of αSYN species (data not shown). Interestingly, the exposure of *PARK2*-variant PD astrocytes to αSYN fibrillar polymorphs mirrored the deleterious effect on mitochondrial function of the *PARK2*-variant PD astrocyte exposed to TNF-α (Figures 4C and 4D).

## DISCUSSION

The specificity of the astrocyte immune reactive responses in PD is poorly understood. For example, it is still unclear if various well-defined species of αSYN that may form in the PD brain can influence the cellular behavior of astrocytes. To investigate astrocyte immune reactivity in PD, we first exposed non-PD human iPSC-derived astrocytes to αSYN assemblies with *in vitro* and *in vivo* seeding propensity (Bousset et al., 2013; Peelaerts et al., 2015). All the tested cytokines showed an elevated response to TNF-α treatment, but there was no increase in cytokine production following exposure to the αSYN species. However, αSYN fibrillar polymorphs triggered changes in the expression of HLA genes encoding MHC class I and II proteins. Moreover, we found the astrocytic immune reactive pro-inflammatory and antigen-presenting phenotypes triggered by TNF-α and αSYN fibrils, respectively, coupled to impaired ATP-generating mitochondrial respiration.

Astrocytic expression of MHC class I and II gene products has been previously reported, and MHC-class-II-positive astrocytes were identified at the edge of lesions in multiple sclerosis brain

**Figure 3. PD astrocytes show functional differences and are prone to release cytokines when treated with monomeric αSYN**

(A) Overview of PD iPSC lines and clones used in this study (1, Holmqvist et al., 2016; 2, Djelloul et al., 2015).

(B) Representative images of alkaline phosphatase (AP)-positive iPSCs used to generate FOXA2 and LMX1A double-positive midbrain progenitors differentiated into S100b and SOX9 double-positive astrocytes. Quantification of S100b- and SOX9-positive astrocytes aged 100 days is shown in graphs in the right panels; data are mean ± SEM; n = 5 or 6 for each variant. Scale bar, 100 μm.

(C) Summary heatmaps of pro-inflammatory cytokine secretion, normalized using total protein (pg/μg protein), in healthy, PARK2, LRRK2, GBA, SNCA, and idiopathic astrocytes following no treatment (NT) or treatment with TNF-α, monomers, ribbons, fibrils, or F110. NT and TNF-α-treated astrocytes were analyzed separately by using unpaired two-tailed Student's t tests; NT and monomer-, ribbon-, and fibril-treated groups were compared using a one-way ANOVA with a Dunnett's multiple comparison test; F110 and remaining forms of αSYN assemblies (not shown) were compared separately using one-way ANOVA with a Dunnett's multiple comparison test; n is shown in (C) and is from 2–3 independent clones with 2–4 differentiations per clone; *p ≤ 0.05; **p ≤ 0.01, #p ≤ 0.001, ##p ≤ 0.0001.

(D) Average total pro-inflammatory cytokine production (pg/μg protein) from PD astrocytes following different treatments. Data are mean ± SEM; n = 3 experiments for 2 to 3 clones used per variant. For each treatment, the variants were compared using a one-way ANOVA with a Dunnett's multiple comparison test; *PARK2*-variant and idiopathic PD astrocytes showed p ≤ 0.05 (*) when compared to non-PD astrocytes (healthy).

(E) Percentage of total cytokine production following various treatments in PD astrocytes.

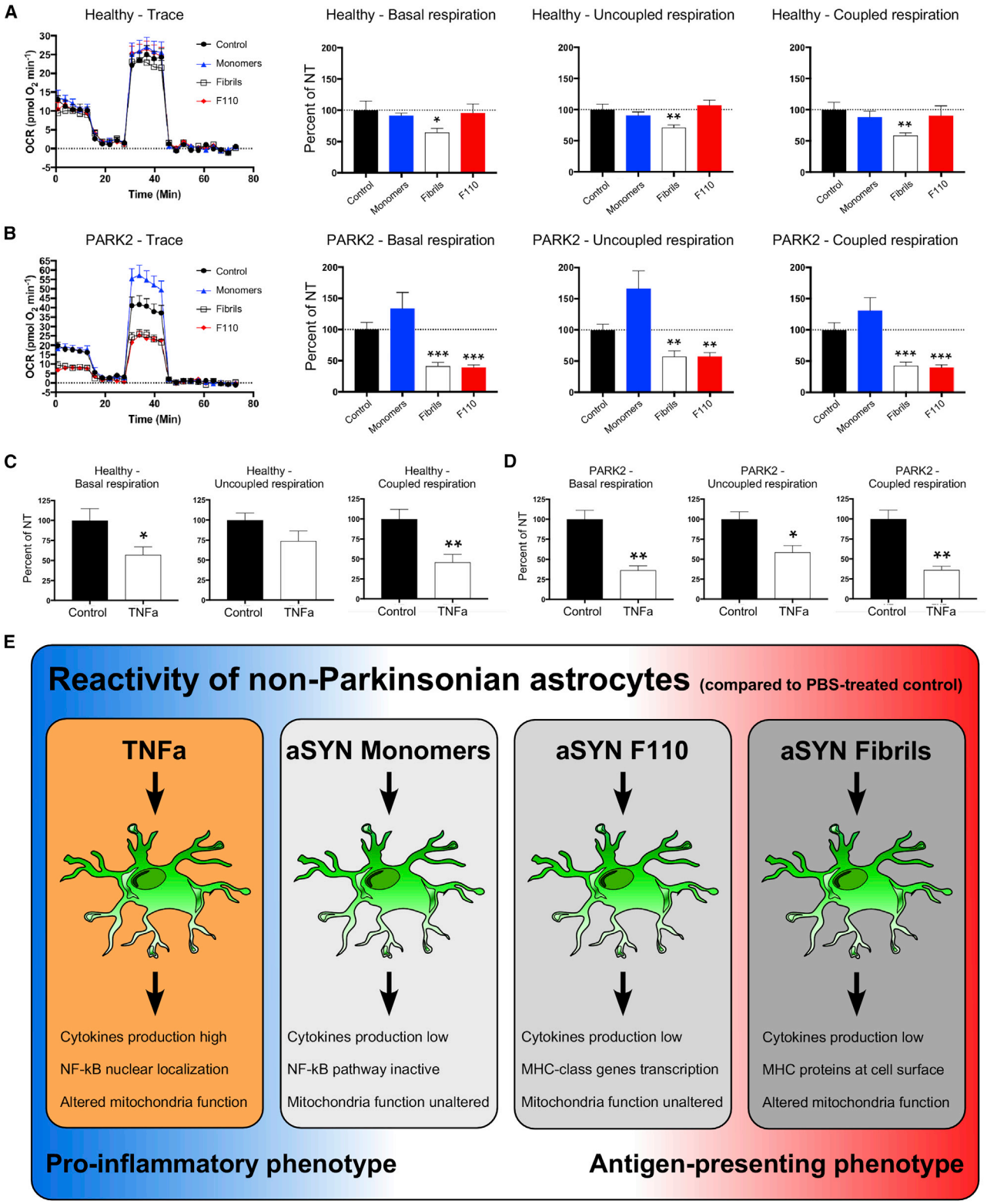



**Figure 4. Mitochondrial respiration impairment in PARK2 variants following αSYN treatment**

(A) Seahorse analysis of mitochondrial respiration following treatment with monomers, fibrils, or F110 in healthy astrocytes showed a significant decrease in uncoupled and coupled citrate-synthase-normalized respiration (depicted as % of NT cells).

*(legend continued on next page)*

tissue (Ransohoff and Estes, 1991; Vardjan et al., 2012). Moreover, astrocytes were shown to phagocytose large neuronal NeuN-positive debris after brain ischemia (Morizawa et al., 2017). Here, we confirmed internalization of fibrillar αSYN polymorphs, which increase expression of an HLA-DMA gene that encodes for the enzyme that facilitate CLIP (class II-associated invariant chain peptide) removal from the MHC class II molecules, allowing them to interact with antigen peptides (Roche and Furuta, 2015), and importantly direct interaction between αSYN fibril peptides and MHC class II proteins in pull-down experiments. Although both fibrils and F110 triggered increased MHC class II gene expression, overlap between MHC class II protein HLA-DPβ1 and αSYN appeared mainly in astrocytes treated with αSYN fibrils. In contrast, HLA-DPβ1 staining was prominent surrounding the large F110 aggregates that had formed prior to being phagocytosed. These data may suggest that temporally accumulated αSYN fibrils in astrocytes were progressively degraded into peptides that bound MHC class II proteins. This was not possible for larger F110 fibril polymorphs that had been phagocytosed. Surprisingly, astrocytes containing αSYN fibrils, overlapping with HLA-DPβ1, almost exclusively relocated MHC class I HLA-F molecules at the astrocyte surface. These data suggested that the astrocytes had adopted an antigen-presenting phenotype, either by cross presentation of αSYN peptides or empty open conformer presentation (Dulberger et al., 2017), similar to oligodendrocytes in a model for multiple sclerosis (Harrington et al., 2020; Kirby et al., 2019). Interestingly, co-treatment of astrocytes with both TNF-α and αSYN fibrils significantly lowered the effect provided by TNF-α or αSYN fibrillar polymorphs alone. Altogether, these data are extremely important as they could imply that the astrocytes' anti-αSYN response could be altered in the presence of pro-inflammatory cytokines and diminished by large aggregates or degradation-resistant fibrils, potentially explaining the permanent increase in αSYN aggregation during disease progression.

αSYN-positive inclusions have been reported in astrocytes from PD post-mortem brains (Braak et al., 2007; Wakabayashi et al., 2000). Moreover, evidence suggests that prolonged astrocytic dysfunction and reactive toxic astrocytes might contribute to the demise of neurons (Kuter et al., 2018; Liddelow et al., 2017). According to our data, healthy astrocytes seem to be able to manage the additional burden of various αSYN species by showing lower total secretion of pro-inflammatory cytokines for most αSYN species. However, the cellular metabolism was altered. Mitochondrial respiration declined in αSYN and TNF-α-treated control astrocytes. This decline was exacerbated in *PARK2*-variant PD astrocytes. These important functional consequences of αSYN fibrils and TNF-α burden might ultimately impact the survival of the neurons, in particular dopaminergic neurons in PD, by diminishing the supportive capacity of the astrocytes. It will be important to further compare the metabolic alterations displayed by astrocytes carrying different variations (e.g., *GBA1* versus *PINK* versus *PARK2*, and other variants).

Our findings highlight various responses of astrocytes to TNF-α and αSYN species and provide insights into the immune reactive role of astrocytes in neurodegeneration. This knowledge could help develop therapeutic approaches to delay the progression of PD and other synucleinopathies.

## STAR★METHODS

Detailed methods are provided in the online version of this paper and include the following:

- KEY RESOURCES TABLE
- RESOURCE AVAILABILITY
  - Lead contact
  - Materials availability
  - Data and code availability
- EXPERIMENTAL MODEL AND SUBJECT DETAILS
  - Ethics
  - iPSC line derivation and production of astrocytes
- METHOD DETAILS
  - iPSC generation
  - Differentiation of iPSCs to astrocytes
  - αSYN purification and species preparation
  - Gene expression analysis
  - Flow cytometry analysis
  - Quantitative RT-PCR
  - Pro-inflammatory cytokine analysis
  - Immunocytochemical analysis
  - Pull-down assay and mass spectrometry
  - Seahorse analysis
- QUANTIFICATION AND STATISTICAL ANALYSIS
  - Statistics
  - Aggregate size counting
  - Bioinformatics

## SUPPLEMENTAL INFORMATION

Supplemental information can be found online at https://doi.org/10.1016/j.celrep.2021.108895.

## ACKNOWLEDGMENTS

We thank AnnaKarin Oldén and Marianne Juhlin for their outstanding technical assistance and the staff at the cytogenetic units at Lund University Hospital for preparing the samples for karyotyping. We are also thankful to the "Cell Line and DNA Biobank from Patients affected by Genetic Diseases" (Istituto G. Gaslini, Genova, Italy) and the "Parkinson Institute Biobank" members of the Telethon Network of Genetic Biobanks funded by Telethon Italy (project no. GTB12001; http://biobanknetwork.telethon.it) for providing fibroblast samples. This work was specifically supported by The Michael J. Fox Foundation; the Swedish Parkinson Foundation (Parkinsonfonden); the Holger Crafoord Foundation; the Thelma Zoegas Foundation; the Shaking Generation

(B) In *PARK2*-variant astrocytes treated with monomers, fibrils, or F110 had a significant effect on basal, uncoupled, and coupled citrate-synthase-normalized respiration (depicted as % of NT cells).
(C and D) TNF-α treatment significantly decreased the basal and coupled respiratory capacity in healthy and *PARK2*-variant astrocytes.
(E) Graphical summary of the overall effects of the various treatments on healthy astrocytes. Seahorse data are mean ± SEM; a t test was used to compare the groups to control; *p ≤ 0.05; **p ≤ 0.01, #p ≤ 0.001, ##p ≤ 0.0001. n = 6–8 technical replicates of 2 biological replicates.

Foundation; the Åke Wibergs Foundation; the Magnus Bergvall's Foundation; the Greta och Johan Kocks Foundation; donations for science, medicine, and technology at Fysiografen in Lund; the Swedish Research Council (grant VR-2015-03684 to L.R.); Brainstem - Stem Cell Center for Excellence in Neurology funded by the Innovation Fund Denmark; and the Olav Thon Foundation in Norway to L.R. The M.V. lab is supported by the Swedish Research Council (grant VR-2015-02510). The R.M. lab was supported by grants from the EC Joint Programme on Neurodegenerative Diseases (JPND-NeuTARGETs-ANR-14-JPCD-0002-02 and JPND-SYNACTION-ANR-15-JPWG-0012-03), the Centre National de la Recherche Scientifique, The Fondation pour la Recherche Médicale (contract DEQ 20160334896), a "Coup d'Elan a la Recherche Francaise" award from Fondation Bettencourt Schueller, the Fondation Simone et Cino Del Duca of the Institut de France, and the European Union (EU/EFPIA/Innovative Medicine Initiative 2 Joint Undertaking IMPRIND grant agreement no 116060; https://www.imprind.org). The L.R. lab is supported by the Strong Research Environment MultiPark at Lund University and the EC Joint Programme on Neurodegenerative Diseases (JPND-MADGIC-VR-2015-06798).

## AUTHOR CONTRIBUTIONS

K.R. designed the study, performed experiments, analyzed data, and wrote the manuscript. G.T. analyzed Affymetrix data. L.B. generated and characterized all biochemically and structurally αSYN forms. S.P. assisted with SeaHorse experiments and data analysis. V.R. performed the mass spectrometry experiment and supervised the pull-down assay. E.S. improved the protocol for generating astrocytes. Y.P. performed generation and characterization of iPSCs. J.S. performed the pull-down assay. T.C.S. performed and analyzed qRT-PCR. C.A. assisted with FACS and αSYN treatment. A.C. performed generation of karyograms and supervision of analysis. S.G. was responsible for provision of study material. K.F. performed data analysis and interpretation. E.E. performed data analysis and interpretation. M.V. performed data analysis and interpretation and editing of the manuscript. R.M. contributed to study design, analysis of data, and editing of the manuscript. L.R. designed study, assisted with generation and characterization of iPSCs, analyzed data, and wrote manuscript. All authors gave input on the manuscript and approved its content.

## DECLARATION OF INTERESTS

The authors declare no competing interests

Received: February 8, 2019
Revised: December 23, 2020
Accepted: March 2, 2021
Published: March 23, 2021

## REFERENCES

Booth, H.D.E., Hirst, W.D., and Wade-Martins, R. (2017). The Role of Astrocyte Dysfunction in Parkinson's Disease Pathogenesis. Trends Neurosci. *40*, 358–370.

Bousset, L., Pieri, L., Ruiz-Arlandis, G., Gath, J., Jensen, P.H., Habenstein, B., Madiona, K., Olieric, V., Böckmann, A., Meier, B.H., and Melki, R. (2013). Structural and functional characterization of two alpha-synuclein strains. Nat. Commun. *4*, 2575.

Braak, H., Sastre, M., and Del Tredici, K. (2007). Development of alpha-synuclein immunoreactive astrocytes in the forebrain parallels stages of intraneuronal pathology in sporadic Parkinson's disease. Acta Neuropathol. *114*, 231–241.

Djelloul, M., Holmqvist, S., Boza-Serrano, A., Azevedo, C., Yeung, M.S., Goldwurm, S., Frisén, J., Deierborg, T., and Roybon, L. (2015). Alpha-Synuclein Expression in the Oligodendrocyte Lineage: an In Vitro and In Vivo Study Using Rodent and Human Models. Stem Cell Reports *5*, 174–184.

Dulberger, C.L., McMurtrey, C.P., Hölzemer, A., Neu, K.E., Liu, V., Steinbach, A.M., Garcia-Beltran, W.F., Sulak, M., Jabri, B., Lynch, V.J., et al. (2017). Human Leukocyte Antigen F Presents Peptides and Regulates Immunity through Interactions with NK Cell Receptors. Immunity *46*, 1018–1029.e7.

Gentleman, R.C., Carey, V.J., Bates, D.M., Bolstad, B., Dettling, M., Dudoit, S., Ellis, B., Gautier, L., Ge, Y., Gentry, J., et al. (2004). Bioconductor: open software development for computational biology and bioinformatics. Genome Biol. *5*, R80.

Ghee, M., Melki, R., Michot, N., and Mallet, J. (2005). PA700, the regulatory complex of the 26S proteasome, interferes with alpha-synuclein assembly. FEBS J. *272*, 4023–4033.

Gribaudo, S., Tixador, P., Bousset, L., Fenyi, A., Lino, P., Melki, R., Peyrin, J.M., and Perrier, A.L. (2019). Propagation of α-Synuclein Strains within Human Reconstructed Neuronal Network. Stem Cell Reports *12*, 230–244.

Gu, Z., Eils, R., and Schlesner, M. (2016). Complex heatmaps reveal patterns and correlations in multidimensional genomic data. Bioinformatics *32*, 2847–2849.

Guerrero-Ferreira, R., Taylor, N.M., Arteni, A.A., Kumari, P., Mona, D., Ringler, P., Britschgi, M., Lauer, M.E., Makky, A., Verasdonck, J., et al. (2019). Two new polymorphic structures of human full-length alpha-synuclein fibrils solved by cryo-electron microscopy. eLife *8*, e48907.

Harrington, E.P., Bergles, D.E., and Calabresi, P.A. (2020). Immune cell modulation of oligodendrocyte lineage cells. Neurosci. Lett. *715*, 134601.

Holmqvist, S., Brouwer, M., Djelloul, M., Diaz, A.G., Devine, M.J., Hammarberg, A., Fog, K., Kunath, T., and Roybon, L. (2015). Generation of human pluripotent stem cell reporter lines for the isolation of and reporting on astrocytes generated from ventral midbrain and ventral spinal cord neural progenitors. Stem Cell Res. (Amst.) *15*, 203–220.

Holmqvist, S., Lehtonen, Š., Chumarina, M., Puttonen, K.A., Azevedo, C., Lebedeva, O., Ruponen, M., Oksanen, M., Djelloul, M., Collin, A., et al. (2016). Creation of a library of induced pluripotent stem cells from Parkinsonian patients. NPJ Parkinsons Dis. *2*, 16009.

Hsiao, H.Y., Chen, Y.C., Chen, H.M., Tu, P.H., and Chern, Y. (2013). A critical role of astrocyte-mediated nuclear factor-κB-dependent inflammation in Huntington's disease. Hum. Mol. Genet. *22*, 1826–1842.

Kirby, L., Jin, J., Cardona, J.G., Smith, M.D., Martin, K.A., Wang, J., Strasburger, H., Herbst, L., Alexis, M., Karnell, J., et al. (2019). Oligodendrocyte precursor cells present antigen and are cytotoxic targets in inflammatory demyelination. Nat. Commun. *10*, 3887.

Kuter, K., Olech, Ł., and Głowacka, U. (2018). Prolonged Dysfunction of Astrocytes and Activation of Microglia Accelerate Degeneration of Dopaminergic Neurons in the Rat Substantia Nigra and Block Compensation of Early Motor Dysfunction Induced by 6-OHDA. Mol. Neurobiol. *55*, 3049–3066.

Lee, H.J., Suk, J.E., Patrick, C., Bae, E.J., Cho, J.H., Rho, S., Hwang, D., Masliah, E., and Lee, S.J. (2010). Direct transfer of alpha-synuclein from neuron to astroglia causes inflammatory responses in synucleinopathies. J. Biol. Chem. *285*, 9262–9272.

Li, B., Ge, P., Murray, K.A., Sheth, P., Zhang, M., Nair, G., Sawaya, M.R., Shin, W.S., Boyer, D.R., Ye, S., et al. (2018). Cryo-EM of full-length α-synuclein reveals fibril polymorphs with a common structural kernel. Nat. Commun. *9*, 3609.

Liddelow, S.A., Guttenplan, K.A., Clarke, L.E., Bennett, F.C., Bohlen, C.J., Schirmer, L., Bennett, M.L., Münch, A.E., Chung, W.S., Peterson, T.C., et al. (2017). Neurotoxic reactive astrocytes are induced by activated microglia. Nature *541*, 481–487.

Loria, F., Vargas, J.Y., Bousset, L., Syan, S., Salles, A., Melki, R., and Zurzolo, C. (2017). α-Synuclein transfer between neurons and astrocytes indicates that astrocytes play a role in degradation rather than in spreading. Acta Neuropathol. *134*, 789–808.

Makky, A., Bousset, L., Polesel-Maris, J., and Melki, R. (2016). Nanomechanical properties of distinct fibrillar polymorphs of the protein α-synuclein. Sci. Rep. *6*, 37970.

Meeuwsen, S., Persoon-Deen, C., Bsibsi, M., Ravid, R., and van Noort, J.M. (2003). Cytokine, chemokine and growth factor gene profiling of cultured human astrocytes after exposure to proinflammatory stimuli. Glia *43*, 243–253.

Morizawa, Y.M., Hirayama, Y., Ohno, N., Shibata, S., Shigetomi, E., Sui, Y., Nabekura, J., Sato, K., Okajima, F., Takebayashi, H., et al. (2017). Reactive astrocytes function as phagocytes after brain ischemia via ABCA1-mediated pathway. Nat. Commun. *8*, 28.

Peelaerts, W., Bousset, L., Van der Perren, A., Moskalyuk, A., Pulizzi, R., Giugliano, M., Van den Haute, C., Melki, R., and Baekelandt, V. (2015). α-Synuclein strains cause distinct synucleinopathies after local and systemic administration. Nature *522*, 340–344.

Pekny, M., and Pekna, M. (2016). Reactive gliosis in the pathogenesis of CNS diseases. Biochim. Biophys. Acta *1862*, 483–491.

Pieri, L., Chafey, P., Le Gall, M., Clary, G., Melki, R., and Redeker, V. (2016a). Cellular response of human neuroblastoma cells to α-synuclein fibrils, the main constituent of Lewy bodies. Biochim. Biophys. Acta *1860*, 8–19.

Pieri, L., Madiona, K., and Melki, R. (2016b). Structural and functional properties of prefibrillar α-synuclein oligomers. Sci. Rep. *6*, 24526.

Poewe, W., Seppi, K., Tanner, C.M., Halliday, G.M., Brundin, P., Volkmann, J., Schrag, A.E., and Lang, A.E. (2017). Parkinson disease. Nat. Rev. Dis. Primers *3*, 17013.

Pomeshchik, Y., Klementieva, O., Gil, J., Martinsson, I., Hansen, M.G., de Vries, T., Sancho-Balsells, A., Russ, K., Savchenko, E., Collin, A., et al. (2020). Human iPSC-Derived Hippocampal Spheroids: An Innovative Tool for Stratifying Alzheimer Disease Patient-Specific Cellular Phenotypes and Developing Therapies. Stem Cell Reports *15*, 256–273.

Ransohoff, R.M., and Estes, M.L. (1991). Astrocyte expression of major histocompatibility complex gene products in multiple sclerosis brain tissue obtained by stereotactic biopsy. Arch. Neurol. *48*, 1244–1246.

Roche, P.A., and Furuta, K. (2015). The ins and outs of MHC class II-mediated antigen processing and presentation. Nat. Rev. Immunol. *15*, 203–216.

Rostami, J., Holmqvist, S., Lindström, V., Sigvardson, J., Westermark, G.T., Ingelsson, M., Bergström, J., Roybon, L., and Erlandsson, A. (2017). Human Astrocytes Transfer Aggregated Alpha-Synuclein via Tunneling Nanotubes. J. Neurosci. *37*, 11835–11853.

Roybon, L., Lamas, N.J., Garcia, A.D., Yang, E.J., Sattler, R., Lewis, V.J., Kim, Y.A., Kachel, C.A., Rothstein, J.D., Przedborski, S., et al. (2013). Human stem cell-derived spinal cord astrocytes with defined mature or reactive phenotypes. Cell Rep. *4*, 1035–1048.

Shrivastava, A.N., Redeker, V., Pieri, L., Bousset, L., Renner, M., Madiona, K., Mailhes-Hamon, C., Coens, A., Buée, L., Hantraye, P., et al. (2019). Clustering of Tau fibrils impairs the synaptic composition of α3-$Na^+/K^+$-ATPase and AMPA receptors. EMBO J. *38*, e99871.

Sloan, S.A., Darmanis, S., Huber, N., Khan, T.A., Birey, F., Caneda, C., Reimer, R., Quake, S.R., Barres, B.A., and Paşca, S.P. (2017). Human Astrocyte Maturation Captured in 3D Cerebral Cortical Spheroids Derived from Pluripotent Stem Cells. Neuron *95*, 779–790.e6.

Sonninen, T.M., Hämäläinen, R.H., Koskuvi, M., Oksanen, M., Shakirzyanova, A., Wojciechowski, S., Puttonen, K., Naumenko, N., Goldsteins, G., Laham-Karam, N., et al. (2020). Metabolic alterations in Parkinson's disease astrocytes. Sci. Rep. *10*, 14474.

Spillantini, M.G., Schmidt, M.L., Lee, V.M., Trojanowski, J.Q., Jakes, R., and Goedert, M. (1997). Alpha-synuclein in Lewy bodies. Nature *388*, 839–840.

Spillantini, M.G., Crowther, R.A., Jakes, R., Hasegawa, M., and Goedert, M. (1998). alpha-Synuclein in filamentous inclusions of Lewy bodies from Parkinson's disease and dementia with lewy bodies. Proc. Natl. Acad. Sci. USA *95*, 6469–6473.

Sun, Y., Hou, S., Zhao, K., Long, H., Liu, Z., Gao, J., Zhang, Y., Su, X.D., Li, D., and Liu, C. (2020). Cryo-EM structure of full-length α-synuclein amyloid fibril with Parkinson's disease familial A53T mutation. Cell Res. *30*, 360–362.

Vardjan, N., Gabrijel, M., Potokar, M., Svajger, U., Kreft, M., Jeras, M., de Pablo, Y., Faiz, M., Pekny, M., and Zorec, R. (2012). IFN-γ-induced increase in the mobility of MHC class II compartments in astrocytes depends on intermediate filaments. J. Neuroinflammation *9*, 144.

Wakabayashi, K., Hayashi, S., Yoshimoto, M., Kudo, H., and Takahashi, H. (2000). NACP/alpha-synuclein-positive filamentous inclusions in astrocytes and oligodendrocytes of Parkinson's disease brains. Acta Neuropathol. *99*, 14–20.

Wang, J., Vasaikar, S., Shi, Z., Greer, M., and Zhang, B. (2017). WebGestalt 2017: a more comprehensive, powerful, flexible and interactive gene set enrichment analysis toolkit. Nucleic Acids Res. *45*, W130–W137.

Wichterle, H., Lieberam, I., Porter, J.A., and Jessell, T.M. (2002). Directed differentiation of embryonic stem cells into motor neurons. Cell *110*, 385–397.

Wickham, H. (2009). ggplot2: Elegant Graphics for Data Analysis (Springer-Verlag, New York).

Windrem, M.S., Osipovitch, M., Liu, Z., Bates, J., Chandler-Militello, D., Zou, L., Munir, J., Schanz, S., McCoy, K., Miller, R.H., et al. (2017). Human iPSC Glial Mouse Chimeras Reveal Glial Contributions to Schizophrenia. Cell Stem Cell *21*, 195–208.e6.

Zhang, Y., Sloan, S.A., Clarke, L.E., Caneda, C., Plaza, C.A., Blumenthal, P.D., Vogel, H., Steinberg, G.K., Edwards, M.S., Li, G., et al. (2016). Purification and Characterization of Progenitor and Mature Human Astrocytes Reveals Transcriptional and Functional Differences with Mouse. Neuron *89*, 37–53.

## STAR★METHODS

### KEY RESOURCES TABLE

| REAGENT or RESOURCE | SOURCE | IDENTIFIER |
|---|---|---|
| Antibodies | | |
| Mouse anti-OCT4; 1:200 | Millipore | Cat# MAB440; RRID:AB_358378 |
| PE-conjugated mouse anti-human NANOG; 1:200 | BD Biosciences | Cat# 560483; RRID:AB_1645522 |
| Mouse anti-TRA-1-81; 1:200 | Thermo Fisher Scientific | Cat# 41–1100; RRID:AB_2533495 |
| PE-conjugated mouse anti-SSEA4; 1:200 | Thermo Fisher Scientific | Cat# A14766; RRID:AB_2534281 |
| Chicken anti-Sendai virus; 1:1000 | Abcam | Cat# ab33988; RRID:AB_777877 |
| Mouse anti-AFP; 1:200 | Sigma-Aldrich | Cat# A8452; RRID:AB_258392 |
| Mouse anti-SMA; 1:200 | Sigma-Aldrich | Cat# A2547; RRID:AB_476701 |
| Mouse anti-B-III-Tub; 1:2000 | Sigma-Aldrich | Cat# T8660; RRID:AB_477590 |
| Rabbit anti-LMX1a; 1:500 | Abcam | Cat# ab139726; RRID:AB_2827684 |
| Goat anti-FOXA2; 1:250 | Santa Cruz | Cat# sc6554; RRID:AB_2262810 |
| Donkey anti-mouse Alexa Fluor® 488; 1:400 | Molecular Probes | Cat# A-21202; RRID:AB_141607 |
| Donkey anti-chicken Alexa Fluor® 488; 1:400 | Jackson Immuno Research Labs | Cat# 703-545-155; RRID:AB_2340375 |
| Donkey anti-mouse Alexa Fluor® 555; 1:400 | Thermo Fisher Scientific | Cat# A-31570; RRID:AB_2536180 |
| Donkey anti-rabbit Alexa Fluor® 555; 1:400 | Thermo Fisher Scientific | Cat# A31572; RRID:AB_162543 |
| Donkey anti-mouse Alexa Fluor® 647; 1:400 | Thermo Fisher Scientific | Cat# A31571; RRID:AB_162542 |
| Donkey anti-rabbit Alexa Fluor® 647; 1:400 | Thermo Fisher Scientific | Cat# A31573; RRID:AB_2536183 |
| Donkey anti-goat Alexa Fluor® 555; 1:400 | Thermo Fisher Scientific | Cat# A21432; RRID:AB_2535853 |
| Rabbit anti-GFAP; 1:100 | DAKO Cytomations | Cat# Z0334; RRID:AB_10013382 |
| Mouse anti-S100b; 1:500 | Sigma-Aldrich | Cat# S-2532; RRID:AB_477499 |
| Rabbit anti-EZRIN; 1:500 | Cell Signaling | Cat# 3145S; RRID:AB_2100309 |
| Mouse anti-EAAT2; 1:500 | Gift from Prof. Jeffrey Rothstein at Johns Hopkins. | N/A |
| Rabbit anti-AQP4; 1:500 | Santa Cruz | Cat# sc-20812; RRID:AB_2274338 |
| Mouse anti-GS; 1:500 | Millipore | Cat# MAB-302; RRID:AB_2110656 |
| Rabbit anti-ID3; 1:500 | Cell Signaling | Cat# 9837S; RRID:AB_2732885 |
| Rabbit anti-NF1A; 1:500 | Active Motif | Cat# 39036; RRID:AB_2335600 |
| Rabbit anti-SOX9; 1:500 | Cell Signaling | Cat# 82630; RRID:AB_2665492 |
| Rabbit anti-GM130; 1:200 | Abcam | Cat# ab52649; RRID:AB_880266 |
| Mouse anti-NF-kB; 1:800 | Cell Signaling | Cat# 6956; RRID:AB_10828935 |
| Mouse anti-HLA-DPb1; 1:500 | Abcam | Cat# ab55152; RRID:AB_944199 |
| Mouse anti-human HLA-DR, DP, DQ; 1:100 | Biolegend | Cat# 361706; RRID:AB_2563192 |
| Mouse anti-O4; 1:100 | Gift from Prof. James E. Goldman at Columbia University of N.Y., USA | N/A |
| Human TruStain FcX; 1:100 | Biolegend | Cat# 422302; RRID:AB_2818986 |
| Rabbit anti-LAMP2A; 1:500 | Abcam | Cat# ab18528; RRID:AB_775981 |
| Mouse anti MHCII beta chain HLA-DPB1; 1:1000 | Abcam | Ab55152 |
| Goat anti-mouse IgG-HRP; 1:5000 | Invitrogen | Cat# A28177 |
| Bacterial and virus strains | | |
| Retroviral vectors; References 1, 2, 3 | | |
| Sendai CytoTune-iPS 2.0; Thermo Fisher Scientific; Cat# A16517 | | |

(*Continued on next page*)

*Continued*

| REAGENT or RESOURCE | SOURCE | IDENTIFIER |
|---|---|---|
| **Chemicals, peptides, and recombinant proteins** | | |
| αSYN species, used at 10 μM, frozen and stored at −80°C until use | CEA and Laboratory of Neurodegenerative Diseases | N/A |
| TNFα, used at 100 ng/ml | PeproTech | Cat# AF-300-01A |
| FGF2 | Thermo Fisher Scientific | Cat# PHG0263 |
| LDN | Stemgent | Cat# 04-0074-10 |
| SB | Selleckchem | Cat# S1067 |
| SHH-C25II | Thermo Fisher Scientific | Cat# PMC8034 |
| CHIR | Sigma-Aldrich | Cat# SML1046 |
| SAG | Millipore | Cat# 566660 |
| FGF8b | Millipore | Cat# PHG0273 |
| EGF | Peprotech | Cat# AF-100-15 |
| Mouse laminin | Thermo Fisher Scientific | Cat# 23017-015 |
| CNTF | R&D Systems | Cat# 450-13 |
| ATTO-488 | Atto-Tec Gmbh | Cat# AD 488-35 |
| ATTO-555 | Atto-Tec Gmbh | Cat# AD 550-35 |
| ECL Femto | Thermo Fisher Scientific | Cat# 34096 |
| Streptavidin Magnetic Beads | Thermo Fisher Scientific | Cat# 88816 |
| Trypsin Gold | Promega | Cat# V5280 |
| EZ-Link-Sulfo-NHS-S-S-Biotin | Thermo Fisher Scientific | Cat# 2133 |
| Seahorse XF calibrant | Agilent | Cat# 100840-000 |
| Seahorse XF-base medium | Agilent | Cat# 103334-100 |
| M-PER extraction reagent | Thermo Fisher Scientific | Cat# 78501 |
| DAPI; 1:10,000 | Life Technologies | Cat# 62248 |
| 7-Aminoactinomycin D (7AAD) | BD Bioscience | Cat# 559925 |
| **Critical commercial assays** | | |
| Fast SYBR Green Cells-to-Ct kit | Thermo Fisher Scientific | Cat# 4402956 |
| TaqMan Fast Advanced Master Mix | Thermo Fisher Scientific | Cat# 4444558 |
| Pierce™ BCA assay | Thermo Fisher Scientific | Cat# 23227 |
| Human Proinflammatory Panel I | MesoScale Discovery | Cat# K15049D |
| EZ-Link-Sulfo-NHS-S-S-Biotin | Thermo Fisher Scientific | Cat# 2133 |
| Protein Assay Kit II | Bio-Rad | Cat# 500-0002 |
| Citrate Synthase Kit | Sigma-Aldrich | Cat# CS0720-1KT |
| Clariom S array | Thermo Fisher Scientific | Cat# 902927 |
| RNeasy Micro Kit | QIAGEN | Cat# 74004 |
| **Deposited data** | | |
| Gene expression microarray data | This study; in supplementary material, as well as at the Roybon laboratory website, section "Resources" | https://www.ipsc-cns-disease.lu.se/ipsc-laboratory-for-cns-disease-modeling/resources |
| **Experimental models: cell lines** | | |
| Irradiated mouse embryonic fibroblasts feeder cells (CF1) | Thermo Fisher Scientific | Cat# A34181 |
| Human induced pluripotent stem cell lines: CSC-9A, CSC-10A/B/C, CSC-7A/B, CSC-21B, CSC-18A, CSC19A, CSC-3G/S. | Reference 1, 2, 3; Roybon laboratory at Lund University, Sweden | N/A |
| Human induced pluripotent stem cell lines: CSC-36D, CSC-37R, CSC-28N, CSC-26B and CSC-27I/K | This study; Roybon laboratory at Lund University, Sweden | N/A |

(*Continued on next page*)

*Continued*

| REAGENT or RESOURCE | SOURCE | IDENTIFIER |
|---|---|---|
| Oligonucleotides | | |
| TaqMan Primer GUSB | Thermo Fisher Scientific | Hs00939627_m1 |
| TaqMan Primer RPL13A | Thermo Fisher Scientific | Hs04194366_g1 |
| TaqMan Primer HSP90AB1 | Thermo Fisher Scientific | Hs04194340_g1 |
| TaqMan Primer HLA-DMA | Thermo Fisher Scientific | Hs00185435_m1 |
| TaqMan Primer HLA-DRB1 | Thermo Fisher Scientific | Hs04192464_mH |
| TaqMan Primer HLA-DPB1 | Thermo Fisher Scientific | Hs03045105_m1 |
| TaqMan Primer CXCL8 | Thermo Fisher Scientific | Hs99999034_m1 |
| TaqMan Primer HLA-F | Thermo Fisher Scientific | Hs04185703_gH |
| Software and algorithms | | |
| FACSDiva v8.0 | BD Biosciences | N/A |
| Prism 7 | GraphPad | N/A |
| Canvas Draw 1.0 | Canvas GFX | N/A |
| R | R Core Team, 2020 | N/A |
| Microplate Manager 5.2.1 | Bio-Rad | N/A |
| Metamorph | Molecular Devices | N/A |
| Other | | |
| Olympus IX-73 inverted microscope | Olympus | N/A |
| Leica TCS SP8 confocal microscope | Leica | N/A |
| C18 Aurora UHPLC column with CSI fittings | Ion Opticks (250mm X 75 μm) | Cat# AUR2-15075C18A-CSI |
| Seahorse XFe96 analyzer | Agilent | N/A |
| BD FACSAria III | BD Biosciences | N/A |
| Ultrasonic processor UIS250v | Hielscher Ultrasonic | N/A |
| Microplate reader Model 680 | Bio-Rad | N/A |
| iMark Microplate reader | Bio-Rad | N/A |
| Nano LC and Mass Spectrometer | EASY-nLC II high performance liquid chromatography (HPLC) system (Proxeon, ThermoScientific, Waltham, MA) coupled to the nanoElute tims TOF Pro (Bruker) | N/A |
| | Separation column: C18 Aurora UHPLC with CSI fittings (250mm X 75 μm, Ion Optiks) | |

## RESOURCE AVAILABILITY

### Lead contact

Further information and requests for resources and reagents should be directed to the Lead Contact, Laurent Roybon (laurent.roybon@med.lu.se).

### Materials availability

iPSC lines generated in this study are biobanked at the CSC Laboratory, at Lund University, Sweden.

### Data and code availability

Microarray and proteomic data are available in Tables S1, S2, and S3, as well as at the Roybon laboratory website (https://www.ipsc-cns-disease.lu.se/ipsc-laboratory-for-cns-disease-modeling/resources). Affymetrix data can be found at NCBI with GSE reference series number: GSE166771 (https://www.ncbi.nlm.nih.gov/geo/query/acc.cgi?acc=GSE166771).

## EXPERIMENTAL MODEL AND SUBJECT DETAILS

### Ethics

All patient biopsies that served to generate the iPSCs were obtained with informed consent and after ethical committee approval at the Parkinson institute in Milan, Italy: Ethics Committee "Milano Area C" (https://comitatoeticoareac.ospedaleniguarda.it/) on the 26/06/2015, and registered under the number: 370-062015. The samples were expanded to generate fibroblasts cell lines and stored at the Telethon genetic biobank (http://biobanknetwork.telethon.it/Pages/View/Documents). The reprogramming of patient samples was regulated by a permit delivered to Dr. Laurent Roybon by the Swedish work environment authority and registered under the number 2020-3211. Work was carried out according to European and Swedish national rules, with the highest level of ethics.

### iPSC line derivation and production of astrocytes

iPSC generation for CSC-9A, CSC-10A/B/C, CSC-7A/B, CSC-21B, CSC-18A, CSC-19A, and CSC-3G/S was previously published (Holmqvist et al., 2016). The same procedure was used to reprogram human epidermal fibroblasts, harvested using a skin punch biopsy from healthy donors CSC-36D and CSC-37R (Pomeshchik et al., 2020), a PD patient with a *SNCA* gene triplication CSC-28N (parent fibroblasts were previously employed to generate the lines CSC-3G and −3S), and two PD patients with idiopathic PD CSC-26B (59 year old female) and CSC-27I/K (47 year old male).

In this study, astrocytes were generated from 74 differentiations in total, all started from pluripotent stem cell stage, from 17 iPSC clones (2-3 clones per donor group) generated from 9 familial and idiopathic PD patients, and 2 healthy individuals. iPSCs were differentiated using a midbrain patterning sequence and expanded as embryoid bodies followed by astrocyte differentiation, expansion, and maturation in adherent cultures to generate mature astrocytes following the outline in Figure 1C. As opposed to previous work (Holmqvist et al., 2015; Roybon et al., 2013), we used a serum-free differentiation protocol as serum exposure may alter the morphology and transcriptome (Pekny and Pekna, 2016; Sloan et al., 2017).

## METHOD DETAILS

### iPSC generation

Briefly, donor fibroblasts were cultured and expanded in Dulbecco's modified eagle's medium (DMEM) supplemented with 10% fetal bovine serum and 1% penicillin-streptomycin (P/S; v/v) at 37°C and 5% $CO_2$ for several passages before being cryopreserved in liquid nitrogen and stored at −150°C. Donor fibroblasts (75,000 cells/well) were plated on 0.1% gelatin-coated 12-well plate and after two days at 37°C at 5% $CO_2$, reprogrammed by use of either retrovirus or non-integration Sendai virus (CytoTune-iPS 2.0) to deliver the reprograming genes *OCT3/4*, *SOX2*, *cMYC*, and *KLF4*). After 7 days of culture, cells were passaged and seeded on irradiated mouse embryonic fibroblasts feeder cells (CF-1 MEF, GlobalStem) with WiCell media composed of advanced DMEM-F12, 20% Knock-Out Serum Replacement (v/v), 2 mM L-glutamine (L-Glu), 1% non-essential amino acids (NEAA; v/v; Millipore), 0.1 mM β-mercaptoethanol (Sigma-Aldrich), and 20 ng/ml FGF2. After 28 days, several clones were isolated and selected based on the morphology of the colonies and seeded onto a MEF-coated 12-well plate with media changed daily and further characterized. The generated lines stained positive for the common nuclear and cell surface pluripotency markers, OCT3/4, NANOG, and TRA1-81 (Figure S1). An alkaline phosphatase (AP) staining was done using the AP staining kit according to manufacturer's protocol (Stemgent), which further confirmed the pluripotency of the iPSC lines (Figure S1). All lines had normal karyotype following a G-banding analysis at 300–400 band resolution on average when testing between passages 8-15 at the Department of Clinical Genetics and Pathology in Lund (Figure S1). All lines were cleared of Sendai virus when tested between passages 8-15 (Figure S1). Genetic integrity was confirmed by fingerprint analysis of isolated DNA from the donor fibroblasts and their respective iPSC line (IdentiCell STR profiling service; Department of Molecular Medicine, Aarhus University Hospital, Denmark). DNA was isolated for direct sequencing using a lysis buffer (100 mM Tris (pH 8.0), 200 mM NaCl, 5 mM EDTA, and 0.2% SDS in distilled and autoclaved water supplemented with 1.5 mg/ml Proteinase K). The presence of the *SNCA* triplication was previously confirmed in our iPSC library study. Lastly, all lines were cultured as EBs and plated on a 96-well plate to demonstrate their ability to spontaneously differentiate into the three germ layers, which was confirmed using immunofluorescent staining with antibodies against B-III-tubulin (B-III-tub), smooth muscle actin (SMA), and α-fetoprotein (AFP; Figure S1).

### Differentiation of iPSCs to astrocytes

On day one of differentiation, human iPSC colonies were harvested, dissociated, filtered (100 μm), and added to an ultra-low-adherent flask (Sigma-Aldrich) with 0.1 μM LDN (Stemgent), 10 μM SB (Selleckchem), 200 ng/ml SHH-C25II (Thermo Fisher Scientific), 0.8 μM CHIR (Stemgent), and 1 μM SAG (Millipore) for 0-4 days in neural induction medium [NIM; advanced DMEM-F12 with 1% L-Glu, 1% NEAA, 1% N2, and 1% P/S (100 U/mL)]. From day 6-8 NIM with 0.1 μM LDN, 0.8 μM CHIR (Stemgent), and 2 μM SAG (Millipore) was used. On day 10, NIM with 0.8 μM CHIR (Stemgent) and 2 μM SAG (Millipore) were used. From days 12-30, NIM with 100 ng/ml FGF8b (Thermo Fisher Scientific) and 2 μM SAG (Millipore) was used. On day 30 EBs were dissociated, filter strained (100 μm), and transferred to a ultra-low-adherent flask containing neural expansion medium [(NEM; DMEM-F12 with 1% L-Glu, 1% NEAA, 2% B27 without vitamin A, 1% P/S, and 0.2 μg/ml heparin (Sigma-Aldrich)] with 20 ng/ml FGF2 (Thermo Fisher Scientific) and 20 ng/ml EGF (Peprotech) for 30 days. On day 60, EBs were washed and dissociated with 0.05% trypsin/1X-EDTA and seeded to

adherent culture flasks coated with 20 μg/ml Poly-L-ornithine hydrobromide (P/O; Sigma-Aldrich) and mouse laminin (15 μg/ml for initial seeding, then 5 μg/ml for subsequently passages) containing NEM and 20 ng/ml CNTF (R&D Systems) for 60-80 days in NDM. Finally, from days 80-100, astrocytes were cultured in neural differentiation medium [NDM; (NB with 1% L-Glu, 1% NEAA, 1% N2, and 1% P/S] with and 20 ng/ml CNTF (R&D Systems). Cells were passaged at confluency. Media was changed every 2 days from day 0-30 and every 3-4 days from day 30-100.

### αSYN purification and species preparation

The expression and purification of human wild-type (WT) αSYN was performed as previously described (Ghee et al., 2005). WT αSYN was incubated in buffer A (50 mM Tris–HCl, pH 7.5, 150 mM KCl) to obtain the fibrillar polymorph "fibrils," in buffer B (5 mM Tris–HCl, pH 7.5) for "ribbons," in buffer C (20mM MES pH6,5, 150mM NaCl) for "F65," and in buffer D (20 mM KPO4 pH9.1) for "F91," at 37°C under continuous shaking in an Eppendorf Thermomixer set at 600 rpm for 4-7 days (Bousset et al., 2013; Makky et al., 2016). A truncated human αSYN spanning residues 1-110 was generated by introducing two stop codons after residue 110 by site directed mutagenesis. This variant was purified exactly as full-length αSYN and was assembled into fibrillar structures "F110" in buffer A. The fibrillar αSYN strains were centrifuged twice at 15,000 g for 10 min and re-suspended twice in PBS at 1.446 g/L. On-fibrillar assembly oligomeric αSYN in PBS was prepared as described (Pieri et al., 2016b). All preformed assemblies as well as monomeric αSYN in PBS were labeled with ATTO-488 (or ATTO-555) NHS-ester (Atto-Tec Gmbh) fluorophore following the manufacturer's instructions using a protein:dye ratio of 1:2. The labeling reactions were arrested by the addition of 1 mM Tris pH 7.5. For fibrillar assemblies, the unreacted fluorophore was removed by a cycle of two centrifugations at 15,000 g for 10 min followed by resuspension of the pellets in PBS. For monomeric and oligomeric αSYN, the unreacted dye was removed using a desalting column (PD10, GE Healthcare) equilibrated in PBS buffer, pH 7.4. The quality control of recombinant human WT αSYN monomeric, oligomeric, fibrillar polymorphs, and F110 was carried out as previously described (Bousset et al., 2013; Makky et al., 2016). For transmission electron microscopy, the assemblies were adsorbed on 200 mesh carbon-coated electron microscopy grids and imaged after negative staining. For fibrillar polymorph fingerprint analysis, aliquots of fibrillar assemblies were removed before or after addition of proteinase K, denatured in boiling Laemmli buffer for 5 min at 90°C, subjected to SDS-PAGE on 12% polyacrylamide gels, and stained by Coomassie coloration. Monomeric and oligomeric αSYN were analyzed by analytical ultracentrifugation (Pieri et al., 2016b). The fibrillar polymorphs were fragmented by sonication for 20 min in 2 mL Eppendorf tubes in a Vial Tweeter powered by an ultrasonic processor UIS250v (250 W, 2.4 kHz; Hielscher Ultrasonic, Germany) to generate fibrillar particles with an average size 42-52 nm.

### Gene expression analysis

Day 97-105 astrocytes were seeded at 300,000 cells/well in a 6-well plate coated with 20 μg/ml P/O (Sigma-Aldrich) and 5 μg/ml mouse laminin for 2 days and treated with either PBS (referred to as non-treated in the study), 100 ng/ml TNFα, or 10 μM αSYN (monomers, fibrils, or F110) for 6 days. Astrocytes were then washed twice with PBS and frozen at −80°C before shipping to Kompetenzzentrum Fluoreszente Bioanalytik (Germany) for gene expression analysis using the Clariom S array (Affymetrix). The total RNA was extracted from dry cells according to RNeasy Micro Kit protocol (QIAGEN). Sample preparation for microarray hybridization was carried out as described in the Affymetrix GeneChip WT PLUS Reagent Kit User Manual (Affymetrix). Summarized probe set signals in log2 scale were calculated by using the GCCN-SST-RMA algorithm with the Affymetrix GeneChip Expression Console v1.4 Software. Average signal values, comparison of fold changes, and significance P values were calculated with R. Probe sets with a fold change above 4-fold (for TNFα-treated samples) and 1.5-fold (for αSYN-treated samples) and a Student's t test *P value* lower than 0.05 were considered as significantly regulated.

### Flow cytometry analysis

Day 97-105 astrocytes were seeded at 500,000 cells/well in a 24-well plate coated with 20 μg/ml P/O (Sigma-Aldrich) and 5 μg/ml mouse laminin for 2 days and treated with either PBS (non-treated), 100 ng/ml TNFα, 10 μM αSYN (monomers, fibrils, or F110), 10 μM αSYN fibril plus 100 ng/ml TNFα, or 10 μM αSYN F110 plus 100 ng/ml TNFα for 6 days. Astrocytes were dissociated using pre-wared Accutase and re-suspended in neural differentiation medium without phenol red. Cells were blocked with 5% donkey serum and TruStain FcX (1:100) for 10 min at RT and then stained for human HLA-DR, DP, DQ (1:100). 7-Aminoactinomycin D (7AAD) was added to detect dead cells and incubated on ice for 5 min prior to analysis. Samples were analyzed using a BD FACSAria III (BD Biosciences) with FACSDiva v8.0 software (BD Biosciences) at the MultiPark Cellomics and Flow Cytometry Core technical platform at Lund University. The cytometer was set up using a 100 μm nozzle at standard pressure of 20 psi and a frequency of 30.0 kHz and was calibrated daily using BD FACSDiva Cytometer Setup and Tracking (CS&T) software and CS&T Research Beads (BD Biosciences). 7-7AAD was excited by the blue laser (488 nm/20 mW) and emission was detected through a 695/40 bandpass (BP) filter. FITC was excited by the yellow/green laser (561 nm/50 mW); emission at 610/20 BP. The strategy for gating was set to separate live and dead cells based on uptake of 7-AAD (data not shown) and FITC-positive cells compared to unstained astrocytes for each treatment condition. Each analysis was based on 10,000 to 20,000 events.

### Quantitative RT-PCR

Day 100-105 old astrocytes were seeded at 18,000 cells/well in a 96-well plate coated with 20 μg/ml P/O (Sigma-Aldrich) and 5 μg/ml mouse laminin for 2 days and treated with either PBS (non-treated), 100 ng/ml TNFα, 10 μM αSYN (monomers, fibrils, or F110), 10 μM

αSYN fibril plus 100 ng/ml TNFα, or 10 μM αSYN F110 plus 100 ng/ml TNFα for 1 or 6 days. Fast SYBR Green Cells-to-Ct kit (Ambion) was used for lysis of astrocytes and reverse transcription to cDNA. The qRT-PCR was done with TaqMan Fast Advanced Master Mix and TaqMan primers (both from Thermo Fisher Scientific) and run according to the manufacture's protocol. $C_T$-values were normalized to the geometric mean of the housekeeping genes *Hsp90AB1*, *GUSB* and *RPL13A* using the $\Delta\Delta C_T$-method. Results were shown as fold change to mean of non-treated samples and a one-way ANOVA with a *P value* of $< 0.05$ was considered significant. Primer ID list and catalog numbers: GUSB (Hs00939627_m1); RPL13A (Hs04194366_g1); HSP90AB1 (Hs04194340_g1); HLA-DMA (Hs00185435_m1); HLA-DRB1 (Hs04192464_mH); HLA-DPB1 (Hs03045105_m1); CXCL8 (Hs99999034_m1); GOLGA8B (Hs00367259_m1); LONP1 (Hs00998407_m1); DNM1L (Hs01552605_m1); HLA-F (Hs04185703_gH).

### Pro-inflammatory cytokine analysis

Day 97-105 astrocytes were seeded at 20,000 cells/well in a 96-well plate coated with 20 μg/ml P/O (Sigma-Aldrich) and 5 μg/ml mouse laminin for 2 days and treated with either PBS, 100 ng/ml TNFα, or 10 μM αSYN (monomers, fibrils, or F110) for 1 hour, 24 hours and 6 days with growth media collected and frozen at −80°C until analyzed. Total protein was determined immediately after growth media was removed and plates for immunocytochemical analysis were immediately fixed (see section below). Total protein from the cell pellet was determined using the Pierce™ BCA assay. M-PER™ extraction reagent was used to lyse cells and the BCA assay was run according to the manufacturer's specified protocol using BSA as a standard and Milli-Q water as blank. Protein samples were analyzed and used to normalize cytokine concentrations. Growth media from astrocytes was quantified using the multiplex pro-inflammatory Panel I (MesoScale Discovery, USA), an electrochemiluminescence sandwich immune-assay, for 10 cytokines including: IFN-γ, IL-1β, IL-2, IL-4, IL-6, IL-8, IL-10, IL-12p70, IL-13, and TNFα. Samples were diluted 1:1 in supplied buffer and analyzed in duplicates according to the manufacturer's specified protocol. Concentrations were normalized using total protein (pg/μg protein). Samples below or above the sensitivity of the assay were set to zero or the max value, respectively. Out of 69 experiments performed, 3 failed and were not included in the analysis (one for GBA, PARK2, and SNCA), as the value for non-treated astrocytes was similar or above that obtained for TNFα-treated astrocytes, which was close to or above the max value of the assay.

### Immunocytochemical analysis

Cell cultures were fixed with 4% paraformaldehyde for 10 min at RT followed by standard immunocytochemical procedures, 1 hour, 24 hours and 6 days post-treatment. Blocking was done in 10% donkey serum in PBS with 0.1% Triton X-100 (Sigma-Aldrich) for 1 h at RT. Primary antibodies, listed below, were added to the wells and incubated overnight at 4°C. Next the secondary antibodies, listed below, were added and incubated for 1h at RT in the dark. Additionally, nuclei were stained by DAPI (1:10,000; Life Technologies). All fluorescent photomicrographs were taken using an inverted epifluorescence microscope (LRI – Olympus IX-73) or confocal microscope (Leica TCS SP8 confocal microscope (Leica Microsystems) equipped with diode 405/405 nm and argon (405, 488, 552, 638 nm) lasers with a HP PL APO 63x/NA1.2 water immersion objective). EBs were taken at day 15 for analysis. They were fixed, sectioned and stained as previously described (Wichterle et al., 2002).

### Pull-down assay and mass spectrometry

Ten million astrocytes were exposed or not to αSYN fibrils labeled with biotin (10 μM) for 6 days. αSYN fibrils in PBS were labeled by addition of 2 molar equivalents of EZ-Link-Sulfo-NHS-S-S-Biotin (Thermo Fisher Scientific #2133) for 1 h at room temperature. The reaction was stopped by addition of Tris–HCl buffer pH 7.5 to a final concentration of 40 mM and incubation during 10 min. The biotinylated αSYN fibrils were recovered by centrifugation, 30 min at 25,000 g at room temperature and resuspended in PBS. The astrocytes were scraped and cytosol and membrane fractions were prepared by incubating the cells with 0.015% digitonin and separating the two fractions by centrifugation (500 g) for 5 min at room temperature. Pull-down experiments were performed on cytosolic and membrane fractions of astrocytes exposed or not to biotinylated αSYN fibrils using streptavidin beads. The presence of MHC-class II proteins within the pull-down was assessed by western blot analysis after PAGE (12% acrylamide) and transfer to nitrocellulose membranes, using the anti-MHC-II beta chain HLA-DPβ1 mouse antibody, the anti-mouse secondary IgG-HRP goat antibody, and ECL Femto (Pierce, Waltham, MA). For mass spectrometry analysis, 250 μg of astrocyte (exposed to biotin labeled αSYN fibrils or not) membrane proteins were loaded onto 90 μl of magnetic beads functionalized with streptavidin (Pierce, Waltham, MA). The pulled down proteins were eluted by 50 μl of Laemmli denaturing buffer, subjected to PAGE and in-gel digested with trypsin Gold (Promega) at a concentration of 10 ng/μl in 25 mM ammonium bicarbonate. The tryptic peptides were dried and resuspended in 10 μl 0.1% trifluoroacetic acid, desalted using a zip-tip C18, eluted, dried and resuspended in TFA. 1μl, corresponding to 250 ng of total proteins, and an equivalent of 1μg of proteins were loaded on the streptavidin beads for the pulled-down fractions were loaded on an C18 Aurora UHPLC column with CSI fittings and the peptides were eluted with a 100 min gradient.

### Seahorse analysis

Mitochondrial respiration was analyzed using the Seahorse XF96 analyzer (Agilent) following the manufacturer's instructions. Briefly, at day minus 9 (−9), 96-well seahorse plates (Agilent) were coated with P/O (20 μg/ml; Sigma-Aldrich) and mouse laminin (5 μg/ml). At day −8, 95-100-day astrocytes were seeded (30,000 cells/well) in 80 μL of NDM with CNTF (20 ng/ml; R&D Systems). At day −6, media was changed and NDM added and cells were either left untreated (PBS condition) or treated with TNFα (100 ng/ml) or αSYN monomers, fibrils, or F110 (10 μM). At day −1, Seahorse XF calibrant (Agilent) was added to hydrate the sensor cartridge

and incubated at 37°C in a $CO_2$-free incubator (Agilent). On the day of the experiment, XF-base medium (Agilent) was supplemented with 5 mM pyruvate (Sigma-Aldrich), 2 mM L-glutamine (Thermo Fisher Scientific), and 10 mM glucose (Sigma-Aldrich) and adjusted to pH 7.4 at 37°C. Cells were washed in XF-base medium (Agilent) and left in a non-ventilated, non-$CO_2$ incubator at 37°C for at least an hour. Oxygen consumption rate (OCR) was measured at baseline (basal) and after sequential additions of 1 μg/ml oligomycin (to inhibit ATP synthase (complex V); measure of coupled respiration), 1 μM FCCP (to uncouple oxygen consumption from ATP production; measure of maximal respiration), and 2 μM rotenone (to inhibit complex I) and 1 μg/ml antimycin A (to inhibit complex III; measure of nonmitochondrial respiration). The FCCP concentration used to measure maximal uncoupled OCR has been determined in a separate set of experiments (data not shown). The average of all data points per respiratory state was used for statistical analysis with exception of FCCP where the data point showing the highest OCR was selected. Following the measurements, the medium was removed and the plate washed with PBS and either PBS or M-PER™ extraction reagent was added to the cells before storage at −20°C for total protein or citrate synthase activity measurements, respectively. The total protein was determined according to the manufacturer's instructions using the Protein Assay Kit II (Bio-Rad) with BSA standard (Bio-Rad) and Milli-Q $H_2O$ as blank. Samples were analyzed and used to normalize Seahorse oxygen consumption rate (OCR). Citrate synthase was determined according to the manufacturer's instructions using a Citrate Synthase Kit (Sigma-Aldrich). Briefly, sample reagent mix was added to each well of the XFe-96 Seahorse plate (Agilent) and the entire well content was transferred to a 96-well plate. Reagent Mix was added to control and samples and background was measured. 10 mM Oxaloacetate Solution was added and citrate synthase activity was determined using a microplate reader. Citrate synthase activity below 1 μmol/ml/min was reanalyzed and if still below 1 μmol/ml/min excluded from the technical replicates. Background values were removed from final measurements. Seahorse analysis was performed with 8 technical replicates from 2 biological replicates. Wells that did not respond to the addition of the drugs were removed from analysis. OCR values were corrected for non-mitochondrial oxygen consumption using the antimycin values. Coupled respiration (respiration linked to phosphorylation by the ATP-synthase) was determined by subtracting the oligomycin OCR from the basal OCR. All values were normalized using citrate synthase activity to show respiratory changes corrected for differences in mitochondrial content of the cells (OCR per CS activity; [pmol $O_2$ $min^{-1}$ / μmol/ml/min]) and displayed as a percent of NT.

## QUANTIFICATION AND STATISTICAL ANALYSIS

### Statistics

Statistical analyses were performed either with GraphPad Prism 7 software or with R (https://www.r-project.org/). Data were presented as mean ± s.e.m. A P value of $< 0.05$ was considered significant. * $p \leq 0.05$; ** $p \leq 0.01$, *** $p \leq 0.001$, **** $p \leq 0.0001$. For the cytokine analysis, 2-3 biologically independent clones with 2-5 differentiations per clone (indicated in the figure or legend) were used. An ANOVA with Dunnett's or Tukey post-test was performed if there were multiple treatment comparisons and time points. A Student's t test was used when comparing a treatment group to the control for the FACS and seahorse experiments.

### Aggregate size counting

The length of the aggregates was measured using the Metamorph software tool "box measurement tool," which produced pixel values that were then converted into length in μm. A total of 75 random ATTO-positive aggregates were counted.

### Bioinformatics

Microarray data handling and analyses were performed using R. We used the gene symbol identifiers of the probes in the gene expression datasets to retain those genes for which there was an Entrez gene identifier using the org.Hs.eg.db package version 3.11.4 available via bioconductor/R, a collaborative open source statistical programming environment (Gentleman et al., 2004). The p value of the filtered data was adjusted for multiple comparison by performing the Benjamini-Hochberg false discovery rate calculation in R. We flagged as significant genes for which the raw p values (sig_p value) were less than 0.05 and less than the corresponding adjusted p value, as previously employed by Windrem and colleagues (Windrem et al., 2017). Heatmaps of gene expression and fold change between condition versus PBS-treated astrocytes were made with ComplexHeatmap version 2.4.3 (Gu et al., 2016). Volcano plots of log P value against log fold change were done using ggplot2 version 3.3.0 (Wickham, 2009). KEGG pathway analysis was performed with WebGestalt version 0.4.4. (Wang et al., 2017).